UNIVERSITY OF COPENHAGEN
FACULTY OF SCIENCE

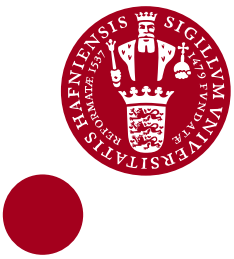

Master Thesis

Polyamorphic systems; An investigation into possiblity of polyamorphic mesostructures previously uncategorised with 2 polymorphs as reference systems.

Author:
Aaron Figus

Supervisor:
Heloisa Nunes Bordallo

Date
22nd of August

Abstract: In this Study we took two different drugs, one we knew to have polymorphs, and one we hypothesized may have polyamorphs. Based on professional criteria and our own findings with the known polymorphic drug, we experimented to determine the possible polyamorphism of our other drug. We found the results to be inconclusive based on the PDF and Activation energy results. It is determined that further testing or possibly a new drug would be necessary to determine the possibility of polyamorphism.

Contents

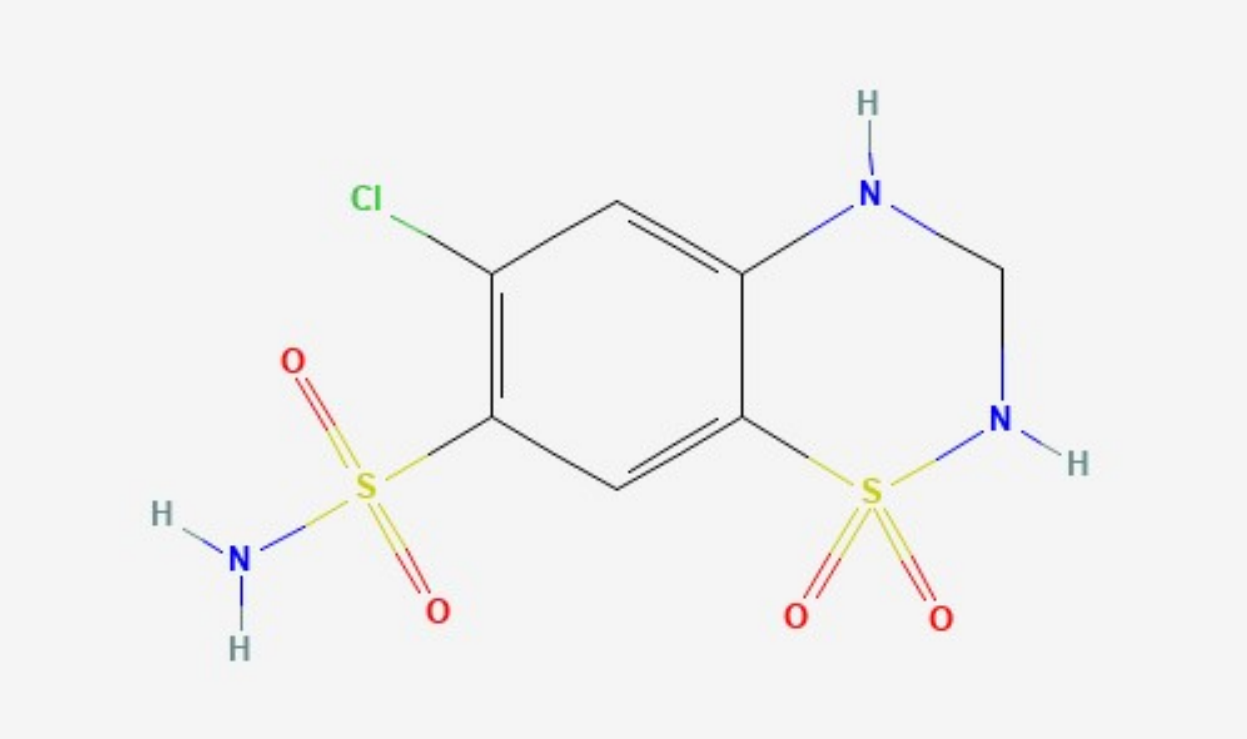

Figure 1: The chemical structure of Hydrochlorothiazide [1]

1 Chapter 1: Introduction

A crystal is defined as "a solid material whose constituents (such as atoms, molecules, or ions) are arranged in a highly ordered microscopic structure, forming a crystal lattice that extends in all directions." [**wikipedia_2022**] Crystals are generally tested using x-ray techniques, as well as thermodynamic measurement, to find characteristic traits distinguishing them. Crystals can also transform into what are known as "amorphous forms" through methods like heating to a melting point, pulverization, and spray drying. An amorphous compound is a compound that has its molecules randomly bonded together with molecular movement occurring, while also being able to hold a shear tension. this ability is what distinguishes an amorphous substance from a liquid. (want to reference but learned this from a conversation with visiting chemistry professor Simon Kimber) This thesis covers two drugs, hydrochlorothiazide (HCT, Fig. 1) and docetaxel (DTX, Fig. 2) which will have their own introductions, that occupy a range of states, from crystalline to amorphous. Broadly speaking, we know docetaxel to have multiple polymorphs, which we plan to test and confirm, and we have taken multiple forms of amorphous hydrochlorothiazide and plan to test the possibility of polyamorphism occurring within the drug. Polymorphism occurrs when you have different possible lattice structures and crystal symmetries for the same compound. This can be due to a number of reasons, such as atmospheric conditions and inclusion of solvents, among other things. The standards to qualify a polymorph differ between fields like pharmacy, academia, and industry.

In industry and pharmacy, a crystal qualifies as a polymorph when: "Demonstration of a nonequivalent structure by single crystal X-ray diffraction is currently regarded as the definitive evidence of polymorphism. X-ray powder diffraction can also be used to provide unequivocal proof of polymorphism. This is summarized in the fluxograms shown in figs. 3, 4, and 5. Other methods, including microscopy, thermal analysis (e.g., differential scanning calorimetry, thermal gravimetric analysis, and hot-stage microscopy), and spectroscopy (e.g., infrared [IR], Raman, solid-state nuclear magnetic resonance [ssNMR]) are helpful to further characterize polymorphic forms."[2]

We will be using this criteria to judge our drugs. This will be done through means of thermal analysis, infrared spectroscopy, x-ray powder diffraction, and Raman scattering. From this study we found that the

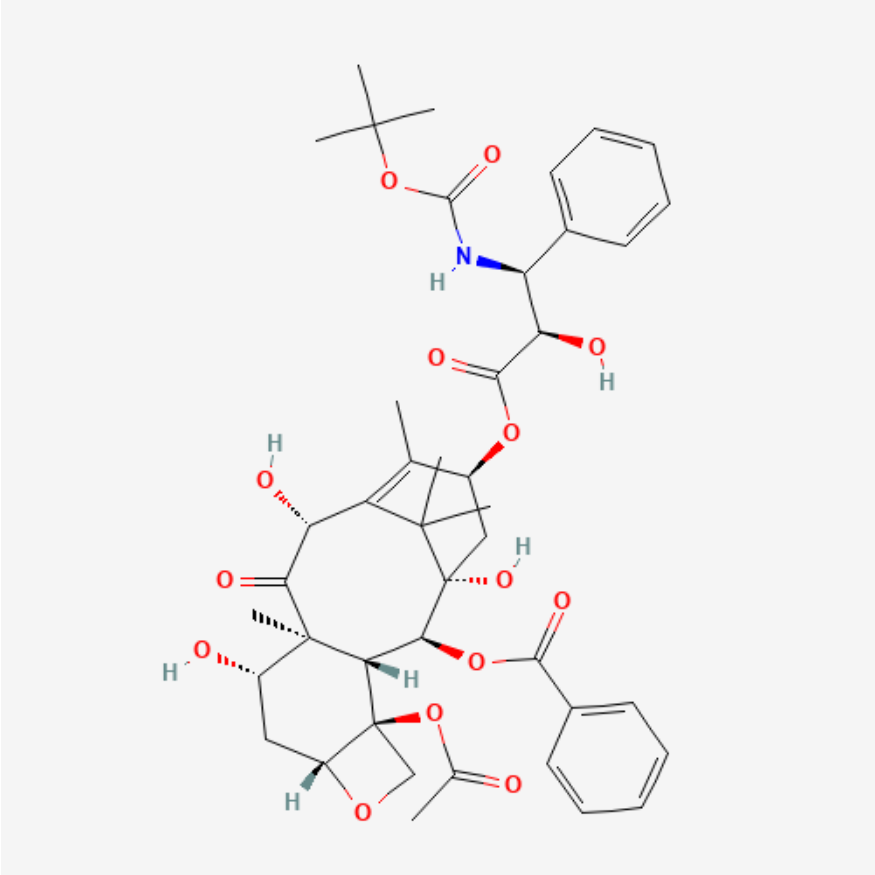

Figure 2: The chemical structure of Docetaxel [**Docetaxel**]

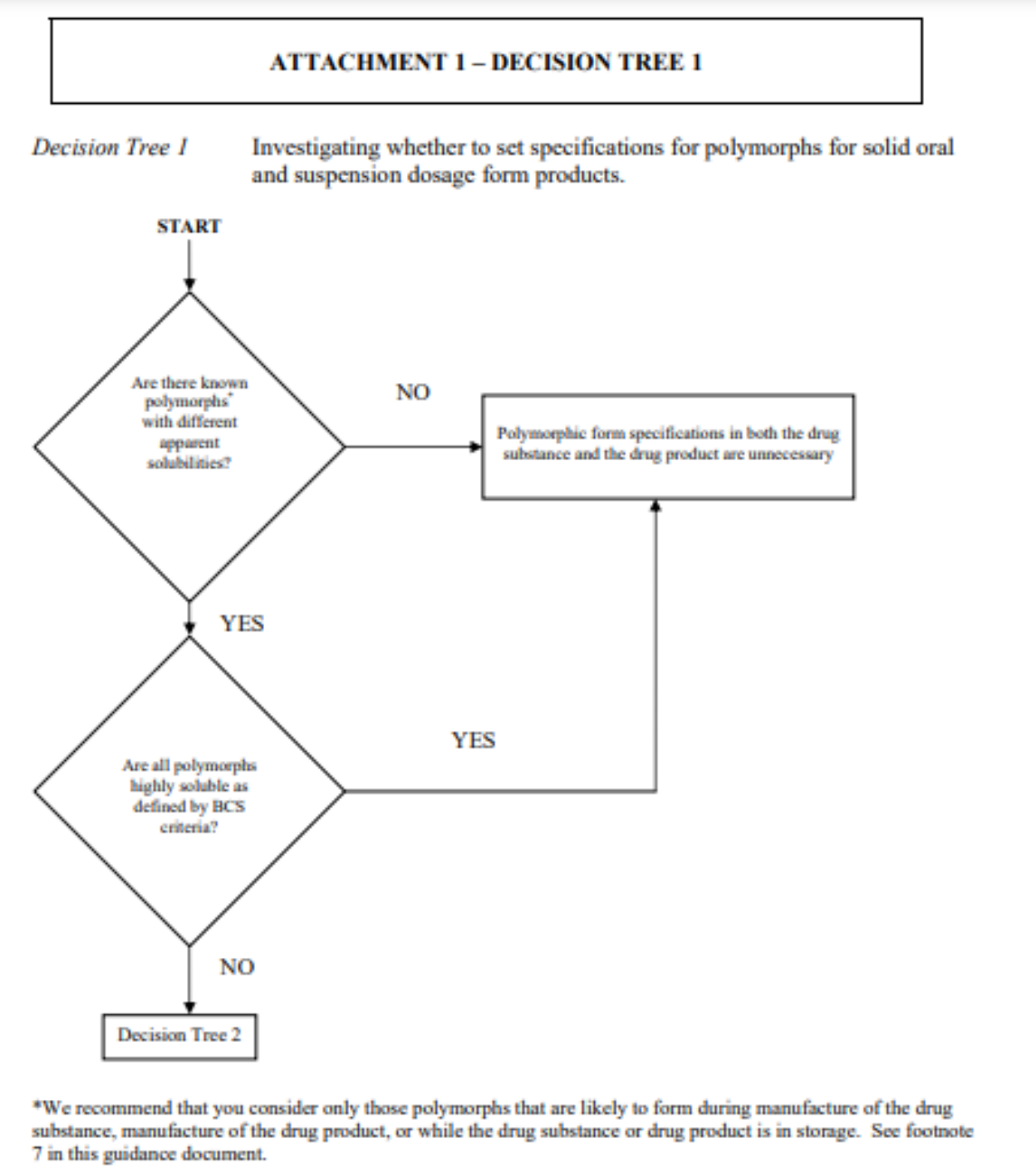

Figure 3: The first of three fluxograms determining whether or not a solid oral and suspension dosage form can qualify as a polymorph and how to categorize.

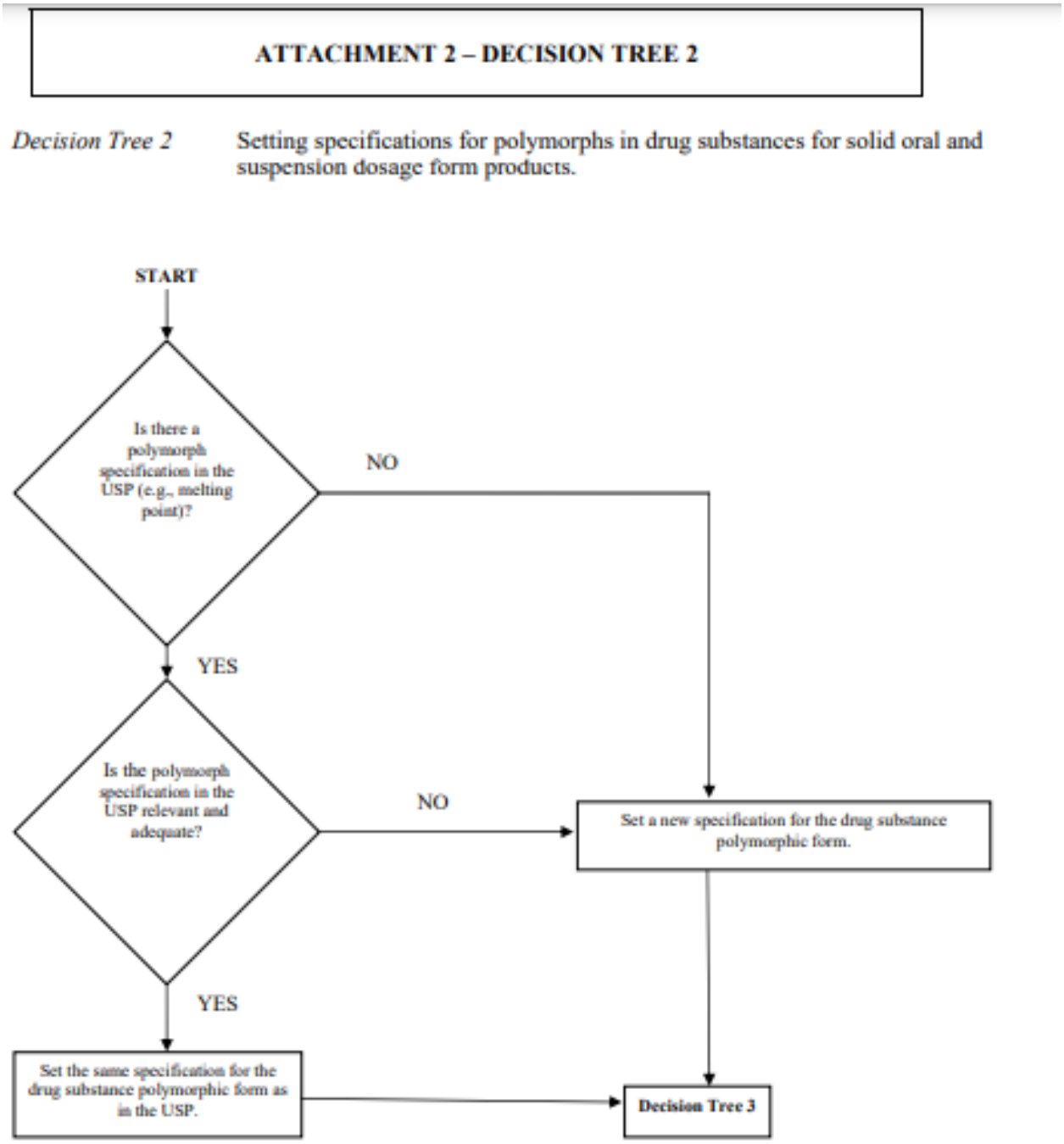

Figure 4: Decision trees for determining whether or not a crystal can qualify as a polymorph and how to categorize.

ATTACHMENT 3 – DECISION TREE 3

Decision Tree 3 Investigating whether to set specifications for polymorphs in drug products for solid oral and suspension dosage form products.

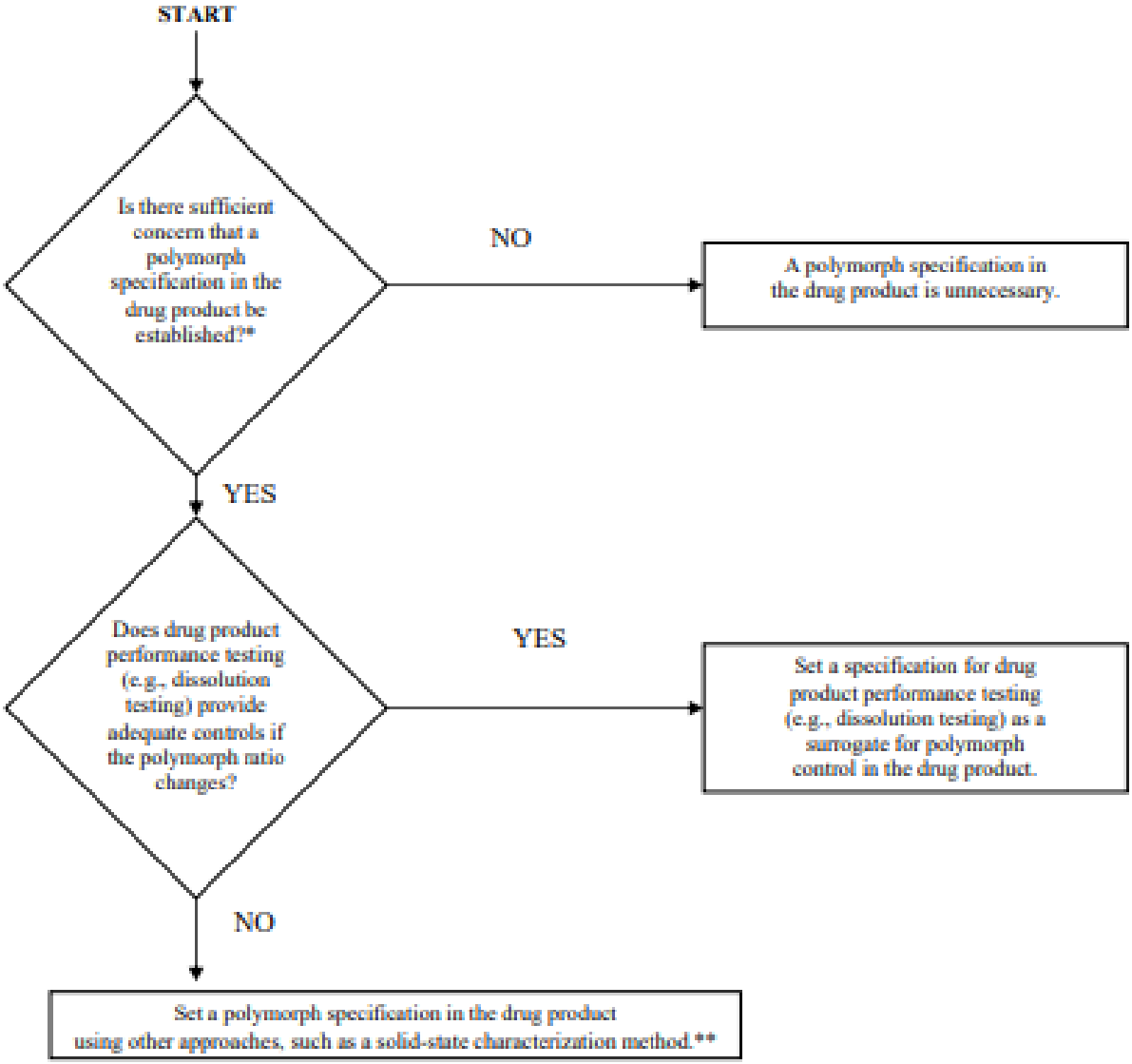

*In general, there may not be a concern if the most thermodynamically stable polymorphic form is used or the same form is used in a previously approved product of the same dosage form.

**Drug product performance testing (e.g., dissolution testing) can generally provide adequate control of polymorph ratio changes for poorly soluble drugs, which may influence drug product BA/BE. Only in rare cases would polymorphic form characterization in the drug product be recommended.

Figure 5: Decision trees for determining whether or not a crystal can qualify as a polymorph and how to categorize.

hydrochlorothiazide forms did not behave in the same polymorphic manner as the docetaxel forms did.

Hydrochlorothiazide, Fig. 1, is a normally crystalline organic compound that is used in pharmaceuticals as a diuretic. Generally, when it comes to pharmaceuticals, the amorphous form of a compound is desired over the crystalline form. This is because an amorphous drug is easier for the body to absorb. The problem is that amorphous substances are not stable, and will recrystallize given enough time. Amorphous substances act a lot like fluids, with the main difference being that an amorphous solid can hold a sheer load, so their molecules are constantly shifting somewhat at random. I've been working with various amorphous forms of HCT to deduce why they have varying thermodynamic properties, most importantly glass transitions. A glass transition occurs when an amorphous substance experiences a sudden change in its derivative thermodynamic properties, going from hard and brittle state to a rubbery consistency as temperature is increased. The more unstable an amorphous substance is, the lower its glass transition. The key to this case is that we have found that all of our amorphous forms have different glass transitions, and when one amorphous form is put through another amorphising process, two glass transitions can be observed in a single measurement. This has never been seen before in any amorphous substance, and we think this may be due to a miscibility gap between the two amorphous states. Our most important question is to figure out what about the different amorphous forms is causing this to happen. My branch of research focuses largely on the thermodynamic differences between each form, and see what dynamics can be observed over the temperature range.

Docetaxel is well-known for its chemotherapeutic properties against breast, prostate, non-small lung, and other kinds of local or metastatic cancer. One of the main issues with Docetaxel is its polymorphism. Due to its different structural appearances, this makes it important, in pharmaceutical perspective, to characterize this drug by means of structural and thermal analysis studies because of the different physicochemical properties arising from such variations in stability and solubility among the different polymorphs. [3]

2 Chapter 2: Methods

2.1 Experimental Methods

2.1.1 Differential Scanning Calorimetry (DSC), [4], [5]

For measuring thermal properties of a material, such as enthalpy of phase transitions of solid or liquid materials, Differential Scanning Calorimetry (DSC) is a very effective and useful tool, and used in many different natural science fields. Some examples of possible phase transitions are: Melting (endothermic reaction, T_m)
Crystallization (exothermic reaction, T_c)
Glass transition (endothermic reaction resulting from amorphism, T_g)
Decomposition/Denaturation (unfolded state, T_d)
The system loses energy in order to keep sample and reference at same temperature, molecules of the material absorb as a result of excess heat brought on by this process, compared to the empty crucible. A melting transition peak to transition of a single molecule, where $\Delta C_p = 0$. Fig. 6

Basically speaking, by measuring change in heat flow that material absorbs/emits during the heating process as a function of time or temperature, the DSC provides results which tell us information about the sample. The data is collected by the measuring cell on top of the furnace, which is where the calorimetric analysis occurs inside of the machine. Within it also is the furnace, heated at a constant rate. This heating is transferred in the thermoelectric disk bases, upon which rest two matching sealed crucibles: one carrying materials (or empty for the correction), and another that's empty acting as a reference sample. The two crucibles are placed on top of and make direct contact with a heating center placed in the bases, which quantifies–thanks to the different heating capacity ΔC_p of the two samples–the heating difference between the samples. The measuring cell of the device consists of all of these parts. Heat flow is then determined by Ohm's Law's thermal equivalent (equation 1):

$$q = \frac{\Delta T}{R} \tag{1}$$

where,

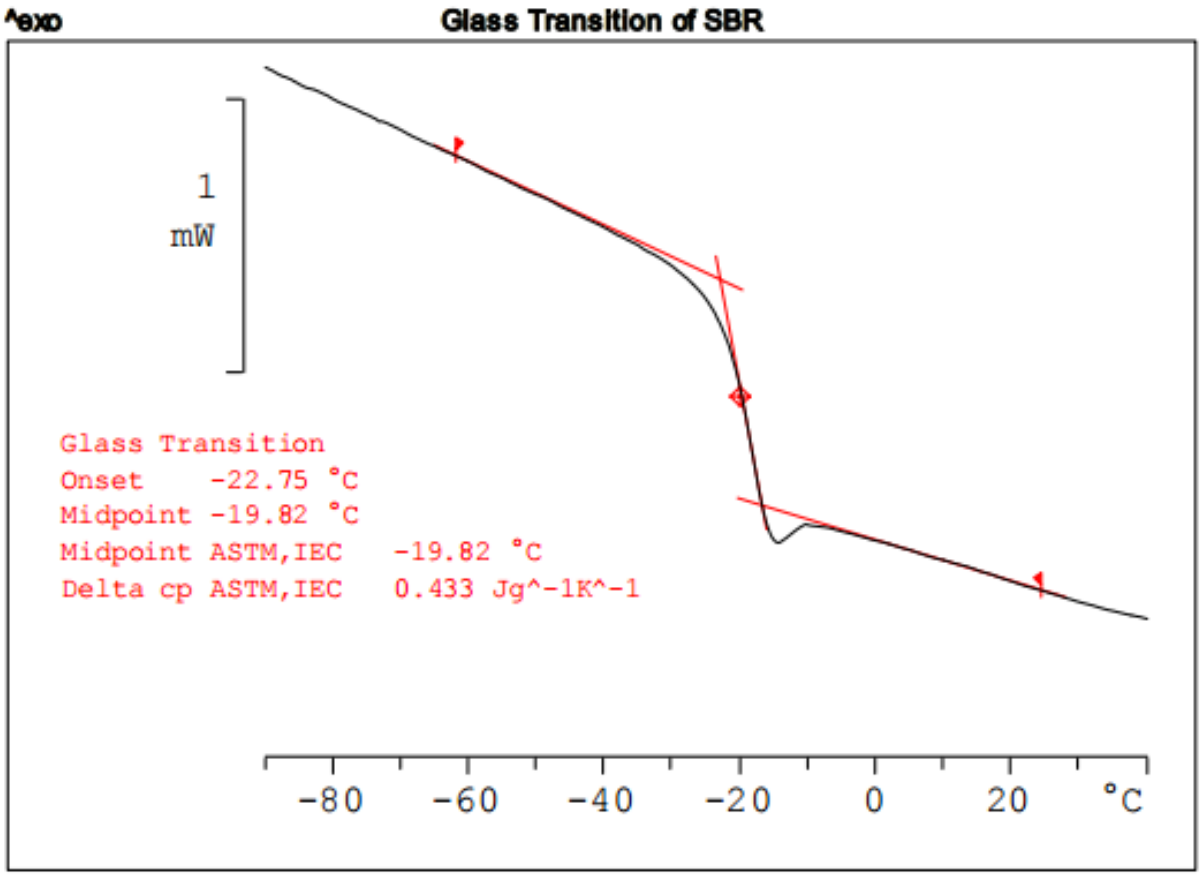

Figure 6: A generic example of a glass transition as detected via DSC. The glass transitions we observe in figure 14 are not as easy to see with the naked eye due to range scale and noise, but this shows the principal of what is graphically happening (a small, broad endothermic reaction). [**mettler-toledo international inc. all rights reserved_2020**]

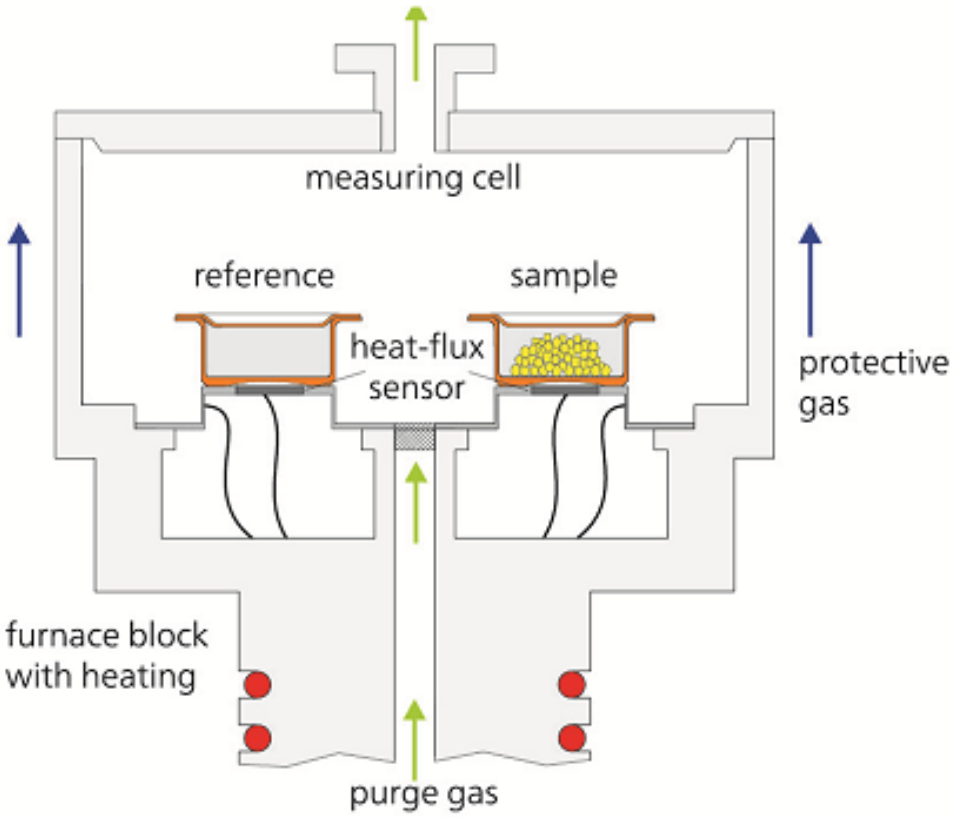

Figure 7: The basic Schematics for a DSC, which works to measure material transitions as a function of time and temperature through [**Gill2010Diffe rentialSC**]

q: heat flow of the sample Δ T: temperature difference between sample and reference R: thermoelectric disk resistance

Integrating the transition area of interest allows us to obtain enthalpy difference, ΔH. We know C_p is the enthalpy's temperature derivative, so (equation 2)

$$C_p = \frac{\Delta H}{\Delta T}_p \tag{2}$$

we can integrate C_p as follows to estimate the enthalpy (equations 3 and 4):

$$\Delta H(T) = \int_{T_0}^{T} \Delta T_p \tag{3}$$

$$\Delta H(T) = \int_{T_0}^{T} C_p(T) dT \tag{4}$$

The instrument used to collect all of these data sets is the DSC 214 Polyma, which features an indium response ratio of over 100 mW/K. Temperature for this instrument is regulated through the use of Nitrogen gas, with our experiments running a PURGE 2 MFC flow of 40 ml/min and a PROTECTIVE MFC flow of 60 ml/min, with a temperature range from -170°C to 600°C. Our heating/cooling rate can range from 0.001 K/min to 500 K/min, and we can achieve a technical resolution of 0.1(mu)W. Our enthalpy precision runs from pm 0.05 % to pm 0.2 % for most samples.

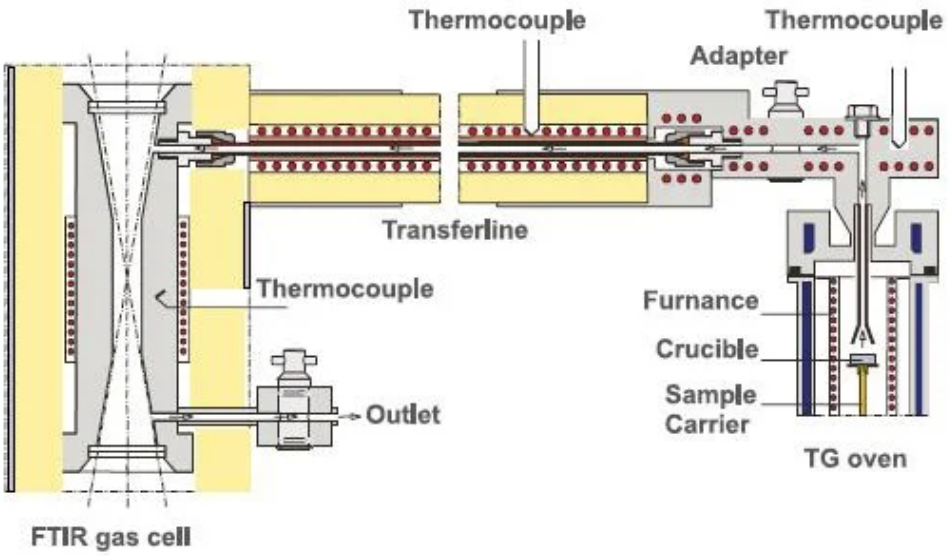

Figure 8: Basic schematics for a TGA, which uses a precision balance to measure changes in mass within a controlled furnace as temperature changes based on a user input temperature program.

2.1.2 Thermogravimetric Analysis Coupled to Fourier-Transform Infrared Spectroscope (TGA-FTIR)

[6] [**margaris_fourier_2014-1**] [7] [8]

The TGA is used to measure the mass loss or gain a sample undergoes as we increase its temperature and decompose it, figure 7. Differences in decomposition temperatures and rates indicate differences in molecular bonds.

This method of measuring material decomposition and/or phase transition is principally, simple. A sample is heated to (and possibly beyond) a decomposition temperature. While it is technically simple, careful measuring conditions throughout the process are required to generate reliable, accurate, and reproducible data.

During a TGA measurement, a sample holder or crucible, is placed on a precision balance-connected plate, which is capable of measuring changes in mass down to hundreds of micrograms (figure 7). While the experiment is ongoing, the plate is held in an electronically programmable furnace which accurately and precisely monitors temperature through an equipped thermocouple.

Due to the basic fact that certain bonds are stronger than others within any molecule, decomposition occurs at different energies (which reads out as temperature in measurement data). We exploit this principle using the TGA by looking at the change in mass during heating. Material starts to lose mass as parts of the molecule break away when required activation energy is reached for the weakest bond. This process starts slowly, with only a few molecules in the sample reaching this required energy at first, but quickly increases in speed as more and more material decomposes. After some time and continued increase in energy beyond the initial decomposition point, the chemical bonds holding these molecules together become very weak. This leads to a drop in rate of mass loss. Subsequently, given sufficient energy, the next bonds begin to break, which leads again to the same sort of mass loss.

We first make a correction measurement consisting of an empty crucible, which serves to generate a background profile at out specified temperature program. The temperature program consists of the heating rate and temperature limit of any sample measurement, as well as any isotherms and emergency shut off

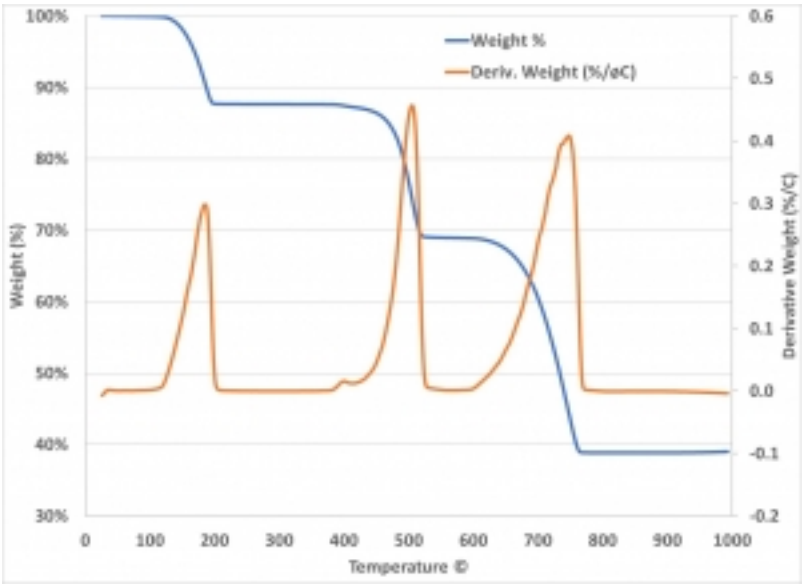

Figure 9: A standard graph of the weight % and derivative weight % of calcium oxalate from 0 to 1000°C. This is a compound that we use to test and calibrate our TGA machine. This is a good way to see how a sample is decomposing on a quantitative scale.

constraints. After all programs are set and crucibles are weighed by the machine, sample can be added. The crucible with sample is then placed into the apparatus and measured according to the previously defined temperature program. As the sample decomposes, any material shed travels upwards as part of a gaseous mixture until it reaches the FTIR spectrometer. The FTIR spectrometer at that point collects the information concerning the composition of the material. This spectroscopic technique is useful for identifying the functional groups present in organic and inorganic compounds through measurement of their infrared radiation absorption over a range of wavelengths [**netzsch**]. The FTIR method first uses an interferometer to collect a sample signal's interferogram, then it performs a Fourier transform on the interferogram to obtain the infrared spectrum. This FTIR spectrum of the material is then finally displayed.[**netzsch**] Rotation or stretching of the interatomic bonds between atoms within the molecule can cause molecules to vibrate in different ways. Depending on the present bonds, these vibrations happen at different wavelengths, which the FTIR coupled to a TGA system can exploit. Infrared light is absorbed when it hits the resonance frequency of the molecules' vibrational modes, resulting in a reduction of intensity of related frequency in a spectrum. The frequency that excites abound state is also dependent upon the bond type and mass of atoms comprising the bond. Thus, the specific molecule changing the infrared signal transmission can be determined. Experimental temperature programs and guidelines will be highlighted in later, drug-specific sections.

We use the Netzsch TG 209 F1 Libra integrated FTIR through the PERSEUS TGA 209 F1 Libra. Temperature regulation is performed through a water bath. Temperature can range from room temperature to 1100°C, with possible heating rates ranging from 0.001 K/min to 200 K/min. We use nitrogen gas so the machine can cool from 1100°C to 100°C in about 12 minutes. The machine is top-loading and can accommodate a maximum sample weight of 2g including crucible. We use Al_2O_3 ceramic open crucibles for our TGA measurements.

2.1.3 Raman Microscope

For HCT and DTX sample scans we used the Renishaw inVia confocal Raman microscope. It operates in a wavelength range of 100 to 3200 cm^-1, and has a spectral resolution and stability of 0.3cm^-1 and $\pm$ 0.01 cm^-1. We use both the 532 and 875nm lasers as detailed in figures 14 and 14.

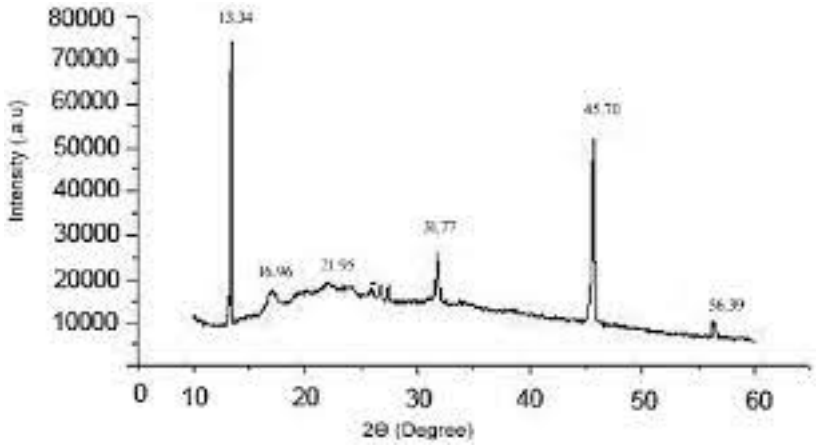

Figure 10: An XRD pattern of a sample compound showing its unique crystalline nature represented by characteristic α and β peaks.

2.1.4 X-ray Powder Diffraction (XRPD)

[9] [**kang_chapter_2016**] [10] [5]

X-Ray Powder Diffraction is one of the most widely used methods for characterising an organic material's crystalline– or in the case of some of our HCT samples, amorphous– structure. X-Rays shone upon a crystal, or crystalline/crystalline capable powdered substances diffract in a pattern characteristic of the structure. This diffraction pattern plots intensity vs angle of the detector, 2θ.

X-Ray Powder Diffraction generally offers greater ease and convenience than single crystal diffraction, largely because it doesn't require the formation of an individual crystal.

Atoms at the surface of a crystal partially scatter X-Rays when they come into contact. The unscattered X-Rays pass through to the next layer of atoms, where they again partially scatter, with remaining X-rays that have not scattered moving to the next layer. This process repeats until the entire crystal has been passed/interacted with. Similar to a diffraction grating, this causes an overall diffraction pattern. Constructive interference (resulting in a visible reflection) occurs when two different layers are in phase, and destructive interference (resulting in a lack of reflection) occurs when two layers are out of phase. A diffraction reflection at any given angle can only occur when Bragg's Law is fulfilled (equation 5):

$$n(\lambda) = 2dsin(\Theta) \tag{5}$$

where,

Θ: diffraction angle of incident X-Ray in degrees

n: diffraction order (integer: n1 = 1, n2 = 2, ...) which counts spacing of crystal layers

λ: wavelength in nm

d: atom layer spacing in nm

The International Centre for Diffraction Data has hundreds of thousands of organic and inorgaanic compounds available through the Powder Diffraction File (PDF)[11]. Because crystalline materials have unique diffraction patterns, the same compound can have polymorphs that are identified by using this pattern diffraction database.

The Basic Powder Diffractometer Powder X-Ray diffractometers consist of an X-ray source (most commonly an x-ray tube), sample holder, detector, and some mechanism for varying angle Theta. The x-ray focuses at an angle θ on the sample, and the intensity of the recieved x-ray at 2θ away from the source path is then read by the detector opposite the source (as seen in figure 10b). The incident angle, which is under the experimentalist's control, is subsequently increased over time while detector angle 2θ remains constant above the source path.

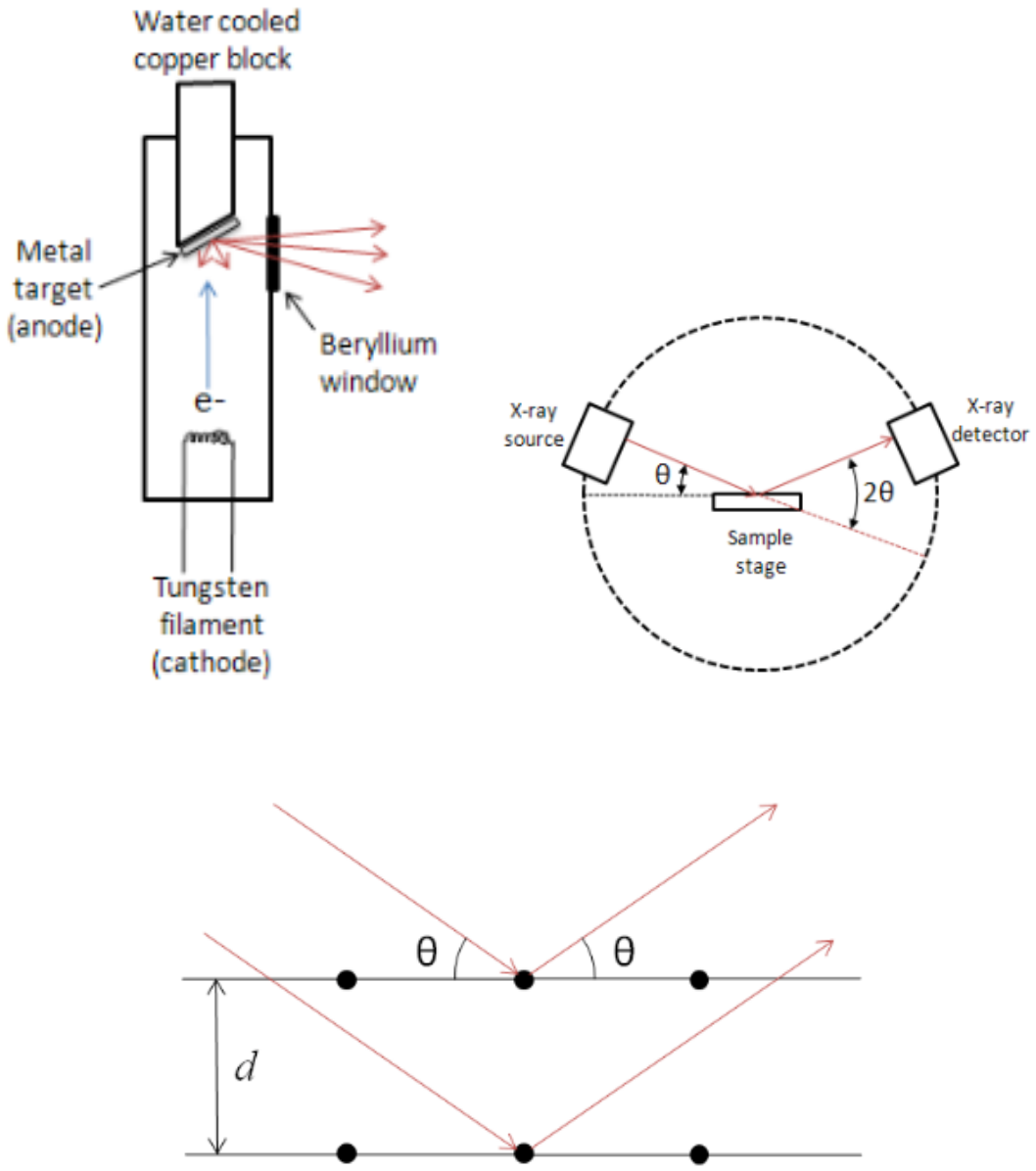

Figure 11: Schematic depictions of the (left, 10a) X-ray tube, where a tungstean filament fires electrons at an angled copper block, causing an ejection of x-rays from the excited copper directed out of a beryllium window; (right, 10b) diffractometer which fires the x-rays from the x-ray tube at a sample at an angle θ, and then measures the scattered rays via a detector located on the other side at angle θ above the horizontal (like the source), allowing us to interpret scattering angle through a 2π revolution up to an angle of 2θ; and (bottom, 10c) the general idea behind generation of a diffraction pattern and reflection if fulfilling Braggs Law (equation 5) where the molecular spacing d in a lattice structure dictates the phase shifts that appear as the Bragg peaks caused by constructive interference (fig. 10).

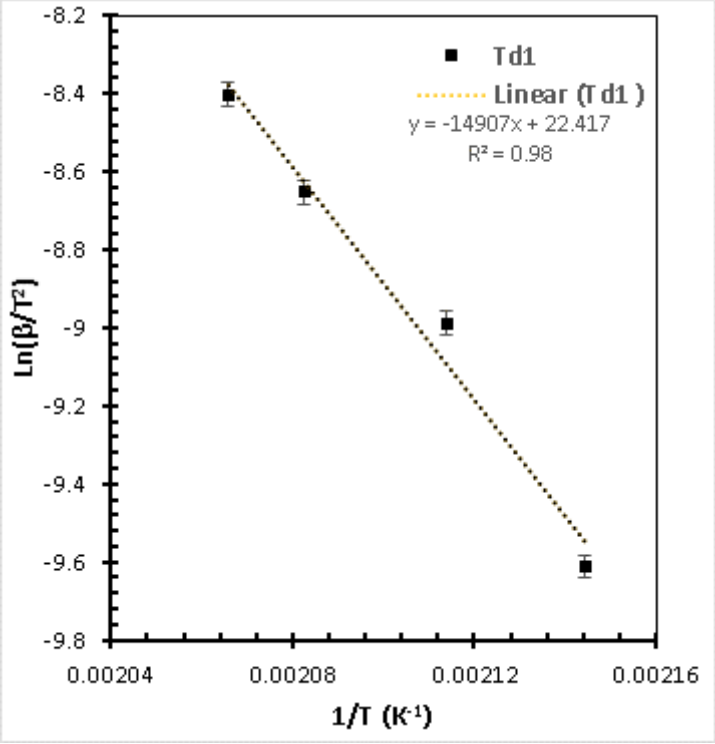

Figure 12: An example of the slope derived from the Kissinger model.

The x-ray tube, evacuated, contains a copper block and tungsten filament with a metal target cathode and anode respectively, with a high voltage between them (figure 10a). A separate circuit heats the filament, and the cathode and anode's large potential difference fires electrons at the metal target. These accelerated electrons collide with core electrons and knock them out of the metal, causing electrons in outer orbitals to drop down and fill the vacancies, emitting x-rays as a result. Those x-rays vacate the tube through a beryllium window. The copper wire is water cooled due to the massive amounts of heat produced by this process.

3 Chapter 3: Kissinger Model and Activation Energy

We will be using the Kissinger method to obtain the kinetic analysis information and estimate activation energy from our observed decompositions. For the sake of brevity, I will not be going into the intricacies of the Kissinger model at this moment. But, in essence, the Kissinger method is a method of differential thermal analysis (DTA) that works by utilizing the principle that thermal decomposition obeys a first order law as well as the Arrhenius equation, and making a number of patterns at different heating rates in order to calculate the kinetic constants directly from the DTA data. So, to do this we have taken data at various heating rates (2.5 K/min, 5 K/min, 7.5 K/min, 10 K/min). All samples were weighted using the TGA's precision balance. [**kissinger_1956**] [**kissinger_1957**]

Interestingly, we could not find the activation energy for HCT using the current data and Kissinger model because it appears a gaussian fit of the dTGA at the temperature range 28 °C to 300 °C cannot be applied. There is no minimum peak for many of the temperature rates as shown in figure 14. The temperature range for these measurements was below the melting (decomposition) point, therefore the Kissinger method could not be applied. One way this can be solved is by increasing the temperature range so that the data has more leeway to form minima peaks.

Table 1: General Hydrochlorothiazide Properties [13]

Melting Point	266-275 $°C$
Decomposition Point	288.31 C (Research)
Boiling Point	576.96 C (TGSC)
Flash Point	302.7 C (Biosynth)
Solubility	10 mM in DMSO; DMSO 60 mg/mL; Water <1 mg/mL
Density	302.7 g/mL
LogP	-1.491

4 Chapter 4: How Did I Get to my Conclusions? (HCT Edition)

4.1 Samples

Table 1 below shows the main physiochemical properties of crystalline HCT. This data was obtained experimentally. [12] [13]

In this project we have been using four forms of hydrchlorothiazide, three amorphous and one crystalline. Our three amorphous forms were a quench cooled form, ball milled form, and spray dried (with ethanol) form. These techniques will be described below. To obtain the comprehensive data needed to form a full picture concerning our polyamorphic forms, we used a variety of thermal, infrared, and x-ray methods to take our measurements.

4.1.1 Crystalline

Our *crystalline form* is unmodified crystallized HCT as received by the research group in Pharmacy.

4.1.2 Quench Cooled

From our crystalline form we can make *quench cooled form* by taking a small portion of our crystalline HCT (1-2 scoops from a laboratory spoon) and placing it onto a flat piece of aluminum foil, doing our best to distribute the powder as one layer. Then we take the entire aluminum "boat" and place it onto a hot plate set to between 280 and 285 C. The HCT is carefully monitored until it melts completely. Once fully melted, but before it burns, the boat is taken off of the hot plate and allowed to cool in a room temperature environment. The sample should be amber in colour. An orange-brown hue means the sample has burned and therefore cannot be used. The cooled, melted sample should now be amorphous, and we gather it by gently scraping the HCT into an eppendorf or small glass flask. Quench cooled samples are generally very stable and can be stored for months without recrystallizing.

4.1.3 Ball Milled

For our *ball milled form* crystalline HCT is placed into a ball mill grinder. This instrument works to blend and/or grind materials through the principles of impact and attrition, where the collision between the ball(s) and the particles reduces particle size to form a powder. For our samples, we use a horizontal vibratory ball mill with stainless steel containers and balls. This is an indirect milling technique, meaning, "the kinetic energy is transmitted to the mill body, and then it is transferred to the grinding medium and charge by friction."[14] This process produces a fine, amorphous, tan-to-brown powder that is about as stable as quench cooled HCT. We gather this by simply pouring and scraping remains into our storage. The coloration is not intended or desired, and likely occurs due to extremely tiny shavings of stainless steel produced through these collisions contaminating our sample. While we find the sample to still be amorphous, it is unlikely that it is completely pure.

4.1.4 Spray Dried

We transform our crystalline HCT into *spray dried form* by the process of spray drying. First we fully dissolve crystalline HCT in ethanol, at a ratio of approximately 2 grams of HCT to approximately 800 ml of ethanol.

Then we would take that solution and run it through one a spray drier located in the pharmacy department. The spray drier would process the HCT by pumping the solution through clean surgical tubing at a user-determined rate. This solution would meet compressed air, filtered in through a programmable aspirator at a preset temperature, and blast through the feed into the drying chamber. From there, the ethanol evaporates as the powder is pulled into a cyclonic tube that deposits into the sample output receptacle. After our sample has been fully processed we remove the output flask and cyclonic tube and scrape from both to obtain our sample. We scrape the sample into glass petri dishes and flasks which we then place uncovered in a dessicator. We scrape the powder from the tube and the powder from the flask into separate containers. This is because in the spray drying process there is a possibility, albeit small, that the sample in one of the receptacles is amorphous, while the other is crystalline. We use silica gel and phosphorous pentoxide, neither of which touch the samples, in the dessicator in order to dry our materials. We allow the sample to dry for about a week before we start withdrawing smaller test samples. The parameters of the spray dryer program are in table 3, and the spray drying equipment schematics are in figure 14.

Table 2: Spray Dryer operating program for HCT

Aspirator	Nitrogen	Inlet Temp.	Pump	Allowable Outlet Temp.
100%	40mg	80 C	15%	~52 C - 55 C

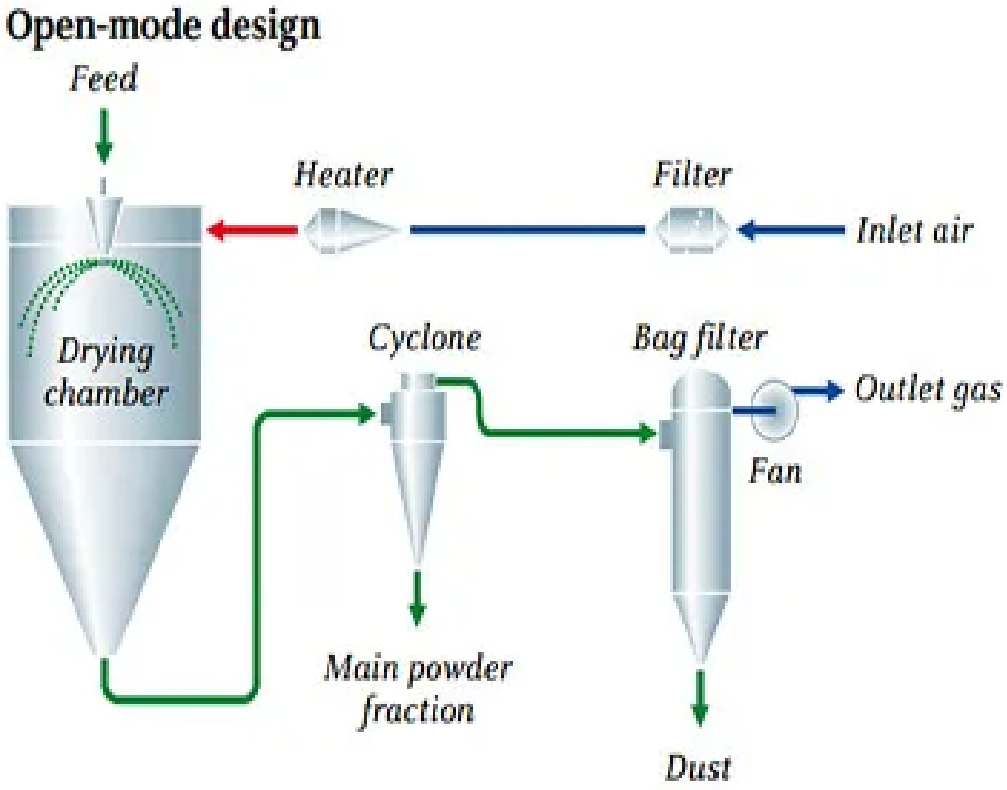

Figure 13: Basic Schematics for an open mode spray drying process. This works by feeding small amounts of homogenous solution, made of sample fully dissolved in a pure organic solvent, into a large drying chamber heated by constantly flowing filtered, heated air where the solvent evaporates. This leaves only amorphous particulate sample to be funneled into the cyclone that deposits the sample into a collector, while the remainder of the flowing air is passed through a bag filter then released through an outlet via fan. (reference direct learning here)

4.1.5 Sample Storage

We store our bulk crystalline HCT in a large flask with a matching lid, and transfer smaller amounts that we plan to use soon into smaller flasks. We do this so if something happens our entire supply is not contaminated. The crystalline sample does not need to be kept air-sealed because there is no danger of the the samples molecular lattice changing while in a resting state over time. The storage methods for the amorphous HCT forms are slightly more complicated. We must keep as little moisture as possible coming in from the environment for our amorphous samples. This is because they are inherently unstable to varying degrees and will recrystallize much more quickly if they become more moist, increase in temperature, or have a large amount of energy suddenly deposited into the system (if the sample faces a hard impact after being dropped for example). To that end, we take some extra cautionary measures with these samples. Our ball mill and quench cooled samples are rather stable, and can last some months in proper storage. In order to protect them, we place our sample into the aforementioned eppendorf/small flask and wrap these (while capped) tightly with parafilm, ensuring as air-tight a seal as possible while still being practical for opening and closing. When used for an experiment, we unwrap the sample storage, withdraw our sample, and then replace with new parafilm. On the other hand, our spray dry samples are very unstable, with a sample made with ethanol lasting a few days or less unless it is under constant desiccation (and even with that, the repeated withdrawal of samples from the desiccator can lead to recrystallization), and samples made with acetone (which we will not be highlighting in this thesis) retaining an amorphous state for less than a day.

Spray dried samples remain uncovered in the desiccator until they are needed for testing. To collect these samples from the larger batch, the desiccator is unsealed and opened and small amounts are withdrawn, these are placed individually in eppendorfs which are then capped and sealed with parafilm. The mother batch is then placed back into the desiccator which is closed and resealed (with dehydrating materials being added to the desiccator environment as needed). At NBI, all amorphous samples are kept in a standard kitchen refrigerator (in the lab at NBI) to slow the crystallization process, while the already crystalline HCT is kept in a capped flask at room temperature. The ball milled and quench cooled samples can be drawn from repeatedly over time for multiple tests with proper storage, but the spray dry samples are one time use. Once the seal is broken and cap is opened on a spray dry eppendorf, the resulting exposure to the environment forces us to use the entire sample in that container quickly. Even just a couple of hours of exposure can facilitate recrystallization. We generally measure these samples first, and set up things like temperature and measurement programs, as well as any autosampling, before opening and placing our spray dry sample into any crucibles or other vessels for this reason.

4.2 Experimental Methods

4.2.1 XRPD

Every time we make a new batch of amorphous samples (of any form), my collaborator Ines C. B. Martins immediately tests a small sample in the Pharmacy Department's XRPD. This is to ensure that we have no crystalline materials remaining to contaminate the batch. Amorphous substances recrystallize much more quickly when in proximity with crystals or crystal nuclei. If she doesn't see any sharp spikes on the XRPD readout at around 16 degrees then we can be confident our sample is amorphous. We do not record this data.

4.2.2 DSC

We used the DSC in order to confirm the glass transitions (Tg) and recrystallization points of our amorphous HCT samples, as well as compare these points (as well as the melting point) and their corresponding enthalpies for all four forms.

4.2.3 TGA-FTIR

Experimental parameters for all HCT data shown in this thesis, for the DSC and TGA respectively, are shown in tables 14 and 14.

DSC Procedures

Sample	Crucible Type	Crucible Mass (mg)	Sample Mass (mg)	Temperature Program
Crystalline	Concavus Al, closed	39.9	2.1	15 minute isotherm, 28C to 350C, 10 K/min
Quench Cool	Concavus Al, closed	39.7	3.2	15 minute isotherm, 28C to 350C, 10 K/min
Ball Mill	Concavus Al, punched	38.6	2.7	15 minute isotherm, 28C to 290C, 2 K/min
Spray Dry	Concavus Al, punched	38.4	2.1	15 minute isotherm, 28C to 300C, 10 K/min

TGA Procedures

Sample	Crucible Type	Sample Crucible Mass (mg)	Initial Sample Mass (mg)	Temperature Program
Crystalline	Al2O3 85 ‘l, open	140.7475	22.1674	15 minute isotherm, 28C to 300C, 5 K/min
Quench Cool	Al2O3 85 ‘l, open	137.8948	11.5338	15 minute isotherm, 28C to 300C, 5 K/min
Ball Mill	Al2O3 85 ‘l, open	139.2335	10.0799	15 minute isotherm, 28C to 300C, 5 K/min
Spray Dry	Al2O3 85 ‘l, open	133.6578	7.6172	15 minute isotherm, 28C to 300C, 5 K/min

Note, not all of the HCT DSC samples undergo the same temperature program. For differences in temperature range, no further consideration is needed because we are only interested in what happens up

to 280 °C. Differences in heating rate will need to be reconciled with further testing because that dictates the amount of energy entering the sample, which can in turn affect glass transition and recrystallization. Ball mill DSC rate was different because at 10K/min heating, it was more difficult to observe the glass transition. I am unsure of why this is the case for the ball mill sample, but not the spray dry sample (which is considerably less stable). Further testing is necessary to understand the cause of this phenomenon.

4.3 Results

Based on the data that I will display below, there are clear thermodynamic differences between our forms. This confirms that there are observable and inherent local bond and alignment differences between the different forms of the sample despite being composed of the exact same molecule.

4.3.1 Differential Scanning Calorimetry (DSC)

Table 3 shows the glass transition, recrystallization, and melting temperatures of amorphous HCT.

Temperature	Glass Transition, Tg °C	Recrystallization Point, Trec °C	Melting Point, Tmelt °C
Crystalline	n/a	n/a	274.0
Ball Mill	116.1	141	267.3
Quench Cool	119.2	183	263.5
Spray Dry	88.7	136	264.2

Table 3: The glass transition, recrystallization, and melting temperatures of our forms.[15]

As we can see in table 3, the glass transition and recrystallization points are higher for the ball milled and quench cooled samples than they are for the spray dried. From this and our prior knowledge of the stability of our different amorphous forms (highlighted in the Materials and Methods section of the thesis), we can infer that the glass transition and recrystallization points are heavily dependent on the stability of the amorphous form. The melting point though, is largely independent of stability, likely because by the time melting temperature is reached, any amorphous HCT form will have recrystallized.

From figure 14 we can see that our amorphous forms all undergo exothermic reactions at points of glass transition (indicated by slight downward bumps in the plot) and recrystallization (indicated by more pronounced drops). This makes sense, since undergoing a glass transition and to an even greater extent recrystallization both fight against chaos in the system to structurally reorganize particles, so energy must be expended. Because the crystalline form is already organized to its most rigid possible extent, it will not undergo an exothermic reaction. All four forms undergo an endothermic reaction upon melting, which happens within a few degrees of each other for all forms, but each form absorbs noticeably different amounts of energy. This seems to indicate there are as of yet unknown differences in the localized order of particles between forms. The drastic fluctuations in the beginning of the measurement (figure 14) are due to instrument stabilization

4.3.2 Thermogravimetric Analysis and IR Spectrum (TGA-FTIR)

There is noticeable difference between the mass losses of all four forms. While the crystalline form retained almost all of its mass until the beginning of decomposition at ≈285 °C, the amorphous forms did not. this makes sense since the stronger bonds of the crystal lattice structure would hinder chemical emission at lower temperatures. The ball milled and quench cooled forms both had a steady overall decline through temperature which became much sharper once decomposition temperatures were reached. Although it is of note that the ball milled form seeming to briefly plateau, if not slightly rise, between 100 °C and 150 °C, indicating that there may have been an absorption at that temperature (which none of the other samples display). The spray dried sample, unlike any of the other forms, experienced a sharp loss in mass early in the temperature program, but then plateaued and maintained that flattened rate of reduction until decomposition. This is possibly because the residual ethanol in the sample, an inherent byproduct of spray drying, is burning off at this temperature. To confirm this theory though we will have to further analyse the specific IR spectra (figs. 18 - 21).

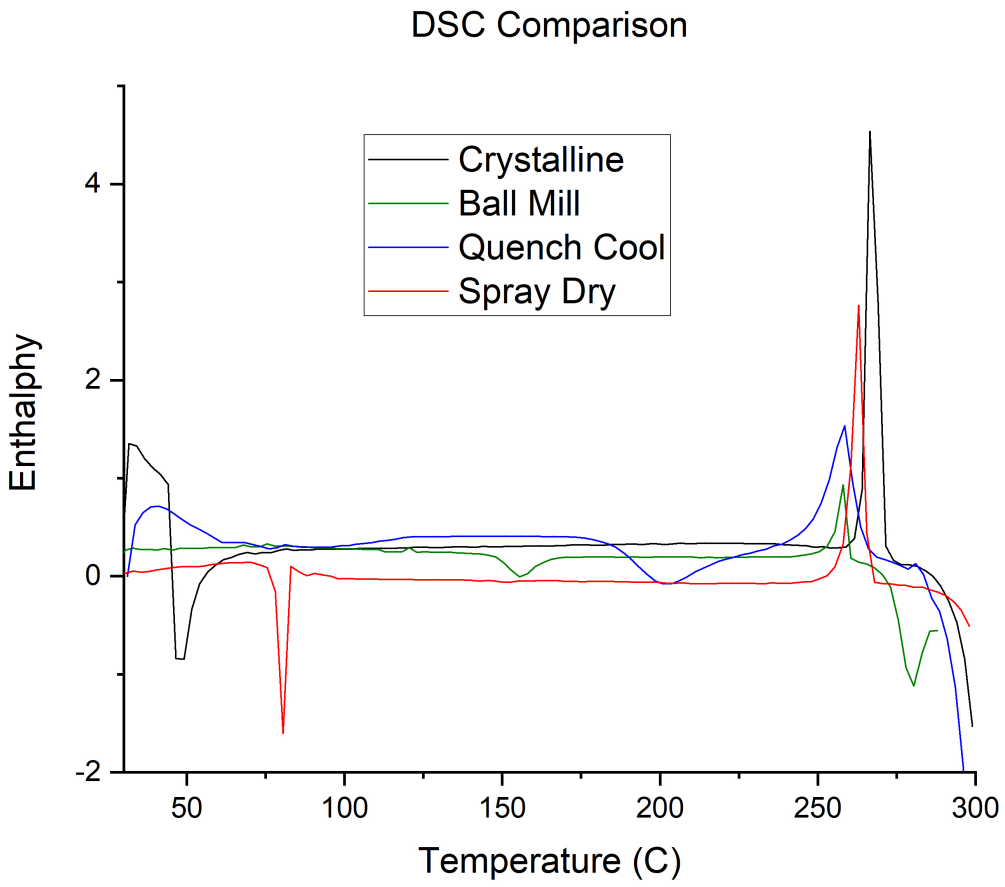

Figure 14: Comparisons of the enthalpy over temperature between all four forms. We can see that the spray dry form has much earlier recrystallisation than the other two forms with the ball mill form having a recrystallisation between the spray dry and quench cooled forms. Obviously the crystalline form does not undergo recrystallisation. There are also slight differences in melting temperature with the order being ball mill $\approx$ quench cool $<$ spray dry $<$ crystalline; and the magnitudes of these melting energy changes increase significantly from ball mill $<$ quench cool $<$ spray dry $<$ crystalline.

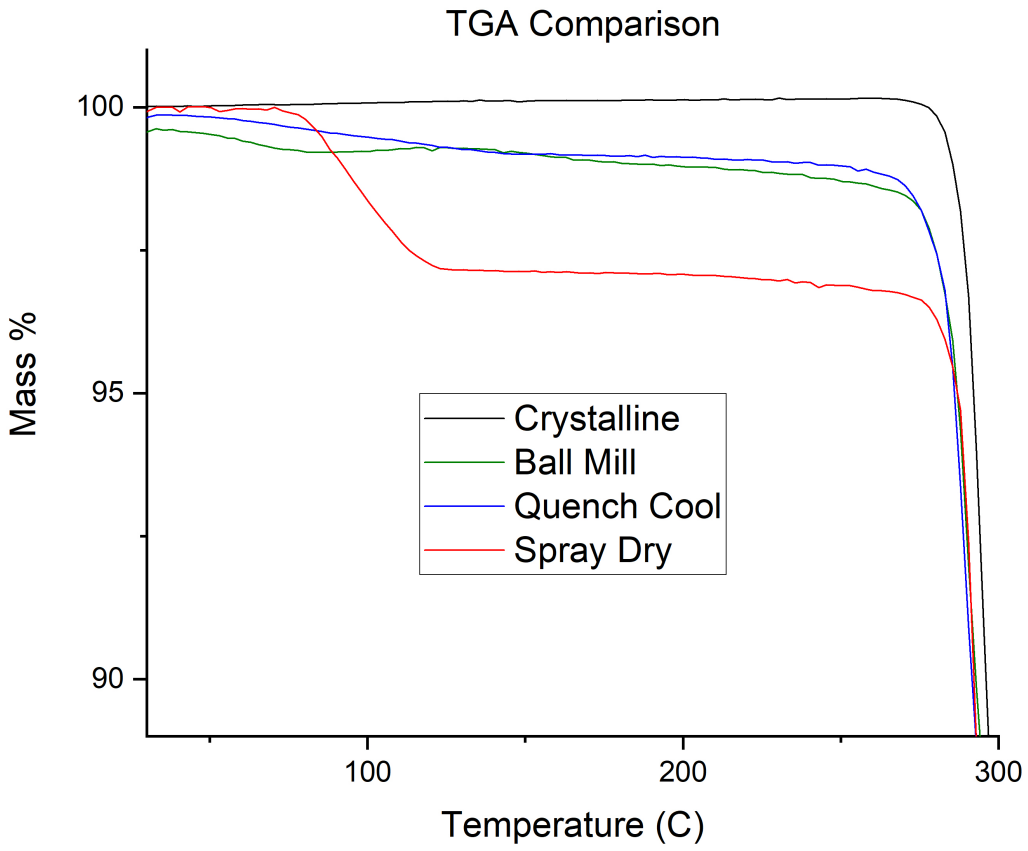

Figure 15: Raw comparison of the mass loss over temperature between all four HCT forms at 10K/min. Spray dry sample shows a marked difference with a steep drop-off in mass from ≈75 °C until plateauing around 100 °C, then behaviour is very similar to crystalline sample until decomposition which occurs around the same temperature (≈280 °C) for all three amorphous samples. The quench cooled and ball milled samples both show steady decline in mass until decomposition. And the crystalline structure shows almost no change until onset of decomposition, a few degrees after the amorphous samples.

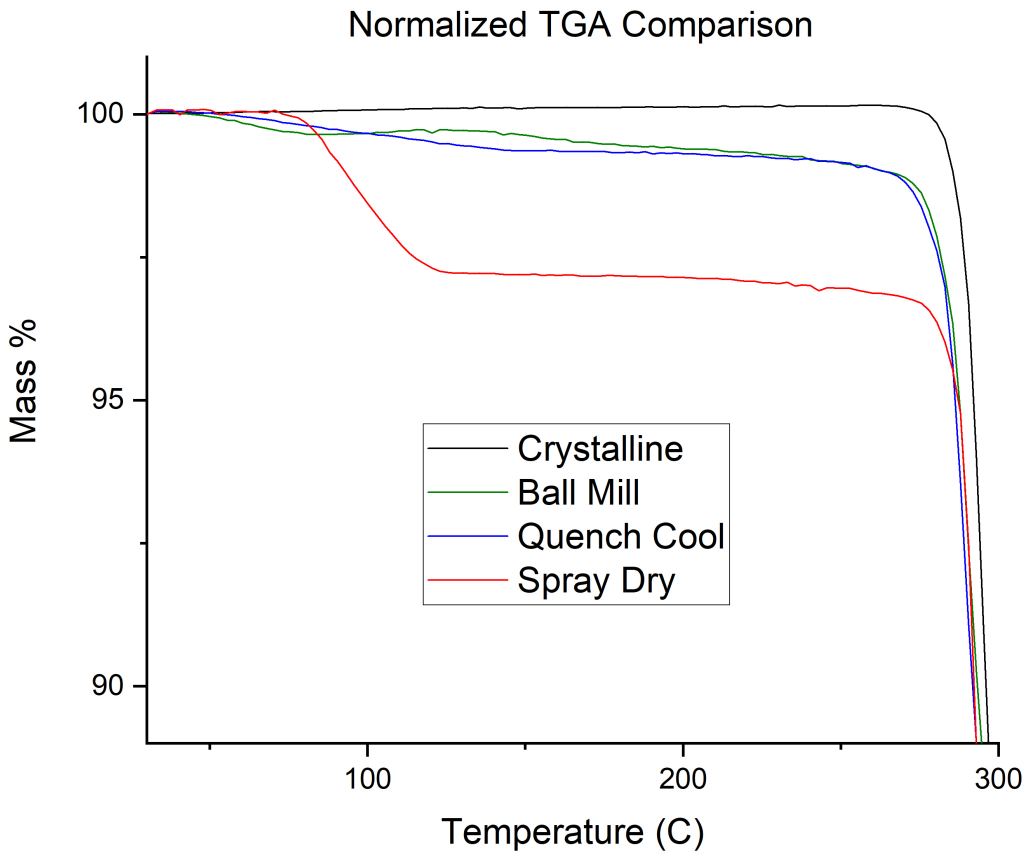

Figure 16: Normalized comparison of the mass loss over temperature between all four forms. Overall behaviour obviously stays largely the same the we can note a small difference in the temperatures where the ball milled and quench cooled samples begin their steady decline, with the ball milled sample beginning emission at a slightly lower temperature than the quench cooled sample.

Table 4: Comprehensive table of all observed mass changes through temperature program

Temperature (C)	Crystalline	Quench Cool	Ball Mill	Spray Dry
50	—	—	H2O	Ethanol
75	—	—	H2O	Ethanol
100	—	—	H2O	Ethanol
125	—	—	H2O	Ethanol
150	—	—	H2O	—
175	—	—	H2O	—
270	—	—	H2O	—
280	Decomposition	Decomposition	Decomposition	Decomposition
290	Decomposition (Shows H-CL)	Decomposition (Shows H-CL)	Decomposition (Does Not show H-CL)	Decomposition (Does Not show H-CL)
299	Decomposition (Shows H-CL)	Decomposition (Shows H-CL)	Decomposition (Does Not show H-CL)	Decomposition (Does Not show H-CL)

We can use the TGA data from figures 15 and 16 to see what temperatures seem the most interesting, and plot them (figs. 18 through 21). We correlate emission to a mass loss, and absorption to a mass gain. Table 4 shows the specific emissions at our selected temperatures, and figures 22(a) through 22(f) show examples of our sample IR spectra vs standard IR spectra for our hypothesized emissions.

By highlighting these specific temperatures for our IR data, we are able to show the rise and fall of different emissions throughout the measurement. If we were to pick completely arbitrary points we could miss something or not see the full breadth of a sample's transformation.

4.3.3 Raman Microscope

Our Raman data seems to tell us that the crystalline and spray dry HCT show Raman Spectra, while the quench cooled form has some peaks but also shows flourescence (fig. 23). The ball milled form shows only flourescence (fig. 23, and this may be because of the impurities. This is interesting since the ball milled form is very powdery, and has impurities much like the spray dry form, but the spry dry form is not flourescent. While it would require further testing, the first thought would be that this fluorescence is due to the metallic shavings that end up mixed into the sample during the ball milling process. (2 separate plots of the flourescent and nonflourescent samples will be placed and explained here)

4.3.4 X-ray Powder Diffraction (XRPD)

I personally was having trouble processing the raw data from our DESY synchrotron trip, so I do not include any plots here. But, through my own in person conversations with the post-doc I was working with from pharmacy, she confirmed that the PDF graph showed all three amorphous forms having no discernible angle shifts in their peaks. This would imply that there are not changes in molecular vibrations between amorphous forms.

5 My Journey to my Docetaxel Conclusions

5.1 Materials and Methods

5.1.1 Samples

5.1.2 Sample Storage

Samples 1-4 (table 6) were stored in 1.5 ml plastic eppendorf containers with attached lids. Lids were kept closed between testing. All samples were kept at room temperature in the dark within the lab.

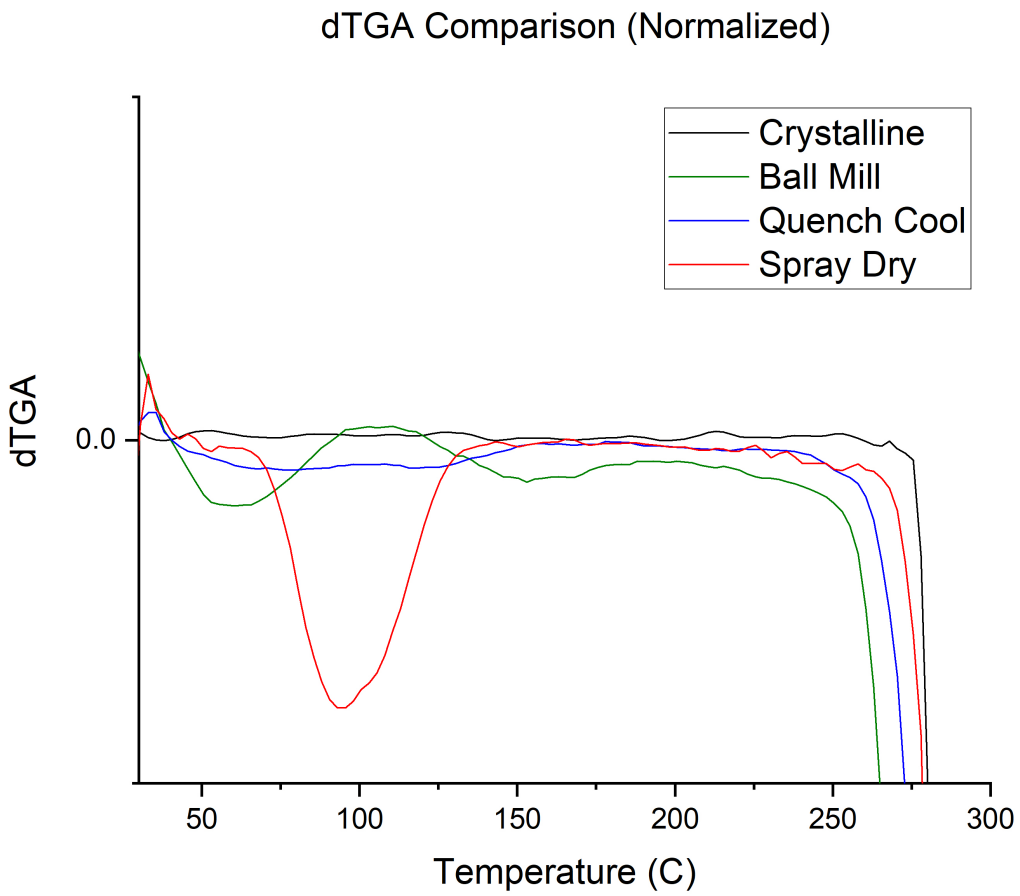

Figure 17: Normalized change in rate of mass loss over temperature, which seemingly supports our findings in table 4

Table 5: General Docetaxel Properties [16]

Melting Point	192-232 $^{\circ}C$
Decomposition Point	186-192 C (Research)
Boiling Point	900.5 C (TGSC)
Flash Point	498.4 C (Biosynth)
Solubility	10 mM in H20; DMSO 25 mg/mL; Ethanol 25 mg/mL; Soluble to 100 mM in DMSO and Ethanol
Density	498.4 g/mL

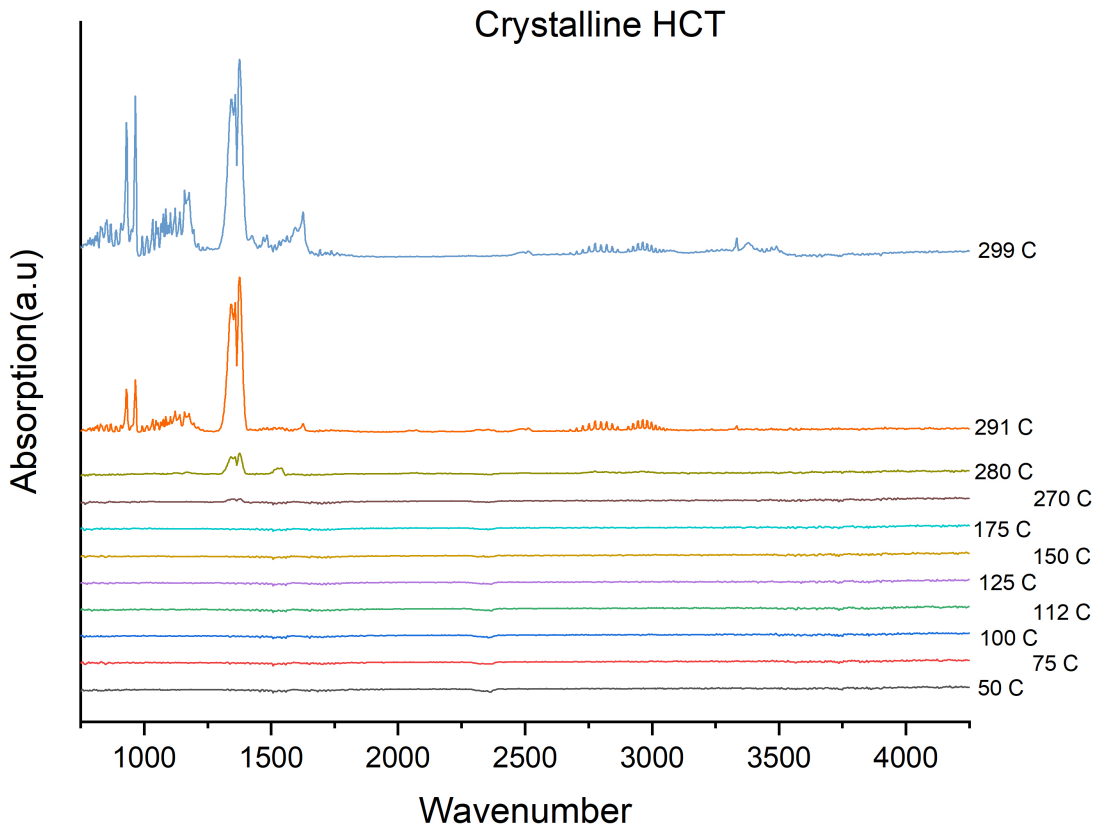

Figure 18: IR spectra of crystalline sample at various temperatures selected from our list of interest

Table 6: Docetaxel Samples

Sample 1	Sample 1; Pure docetaxel sample (having undergone an X-ray treatment) 1-2 years old at time of measurement
Sample 2	Sample 2; Pure docetaxel sample 1-2 years old at time of measurement
Sample 3	Sample 3; Treated docetaxel sample (previously cooked to 65C and X-rayed) 1-2 years old at time of measurement
Sample 4	Sample 4; Unknown docetaxel polymorph fresh
Sample 5	Data only; FTIR data collected by Nikos Giannoulis in 2020-2021 on his pure docetaxel sample (sample 2 today) [**giannoulis_2021**]

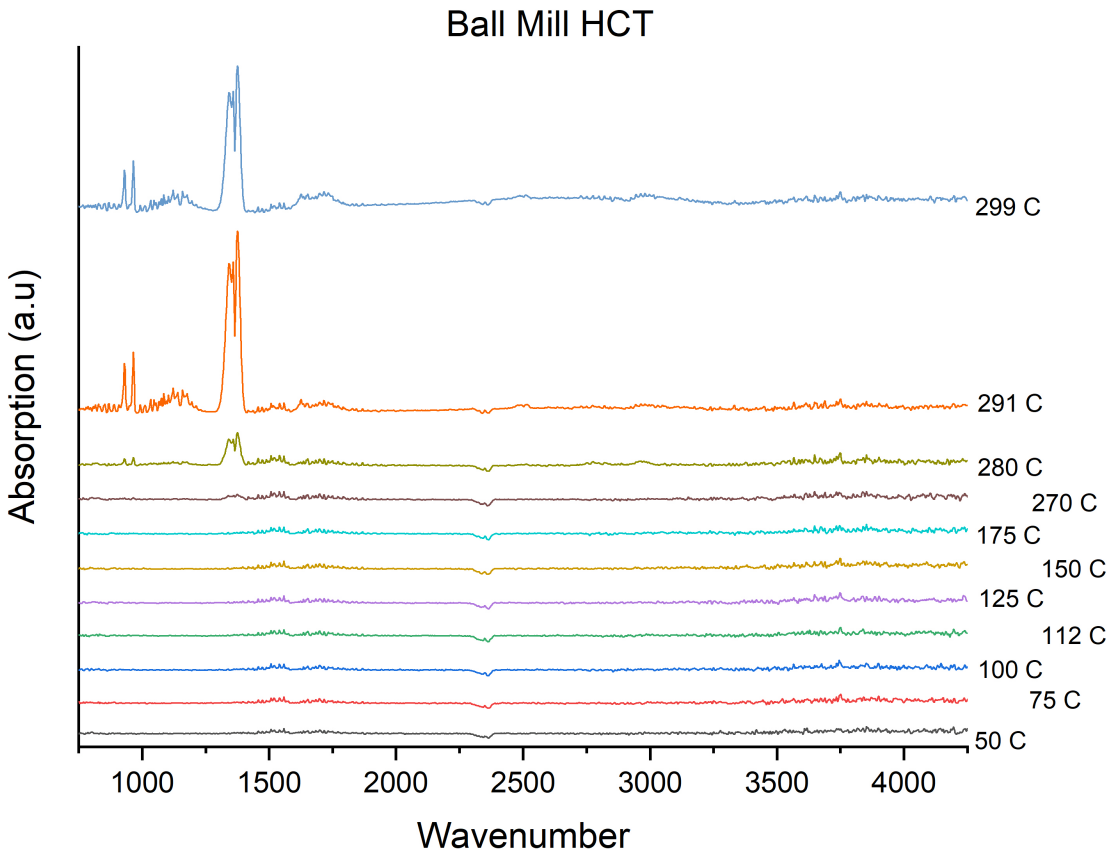

Figure 19: IR spectra of ball milled sample at various temperatures selected from our list of interest

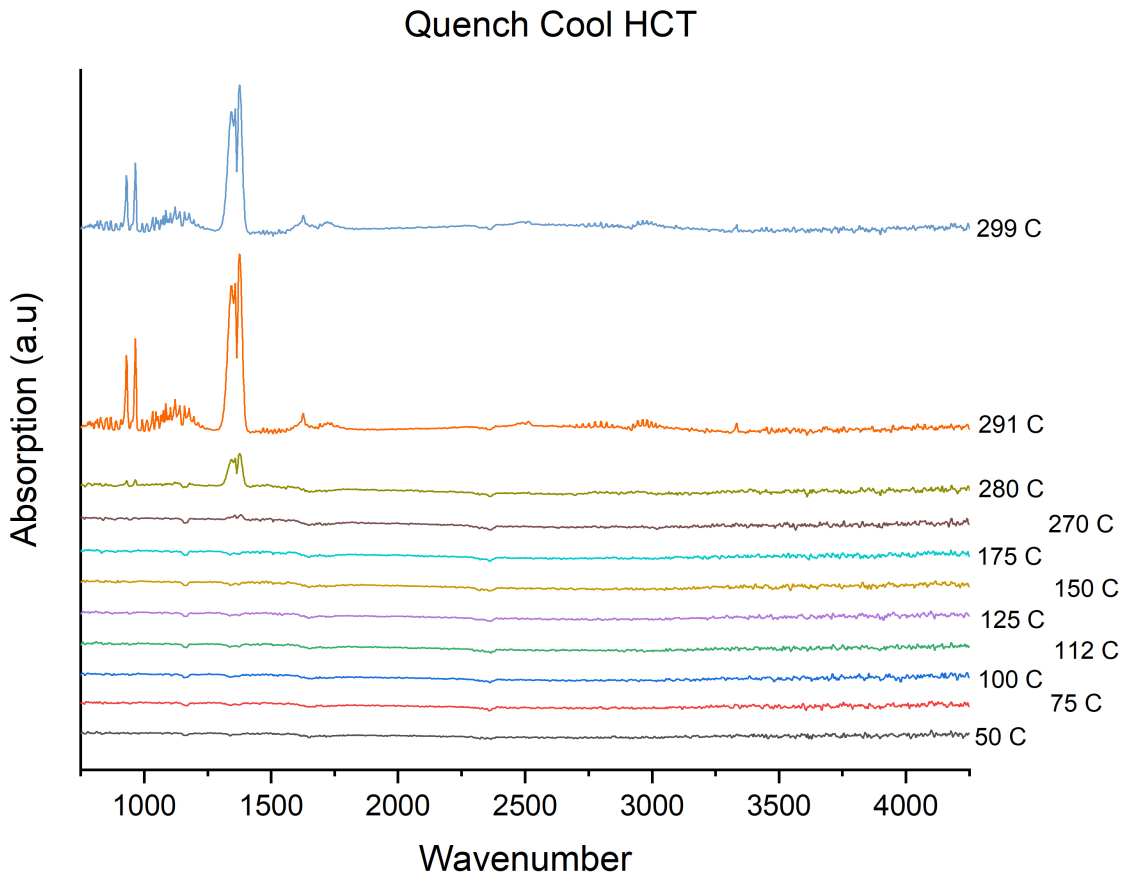

Figure 20: IR spectra of quench cooled sample at various temperatures selected from our list of interest

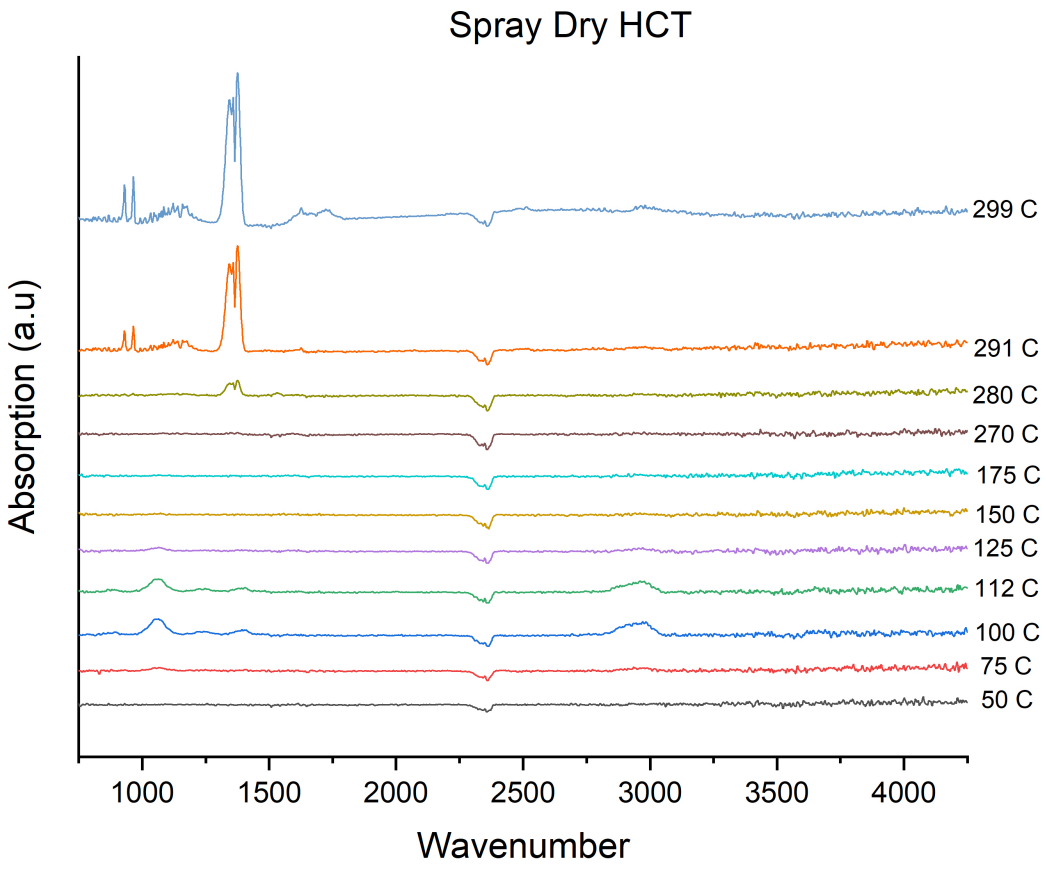

Figure 21: IR of spray dried sample at various temperatures selected from our list of interest

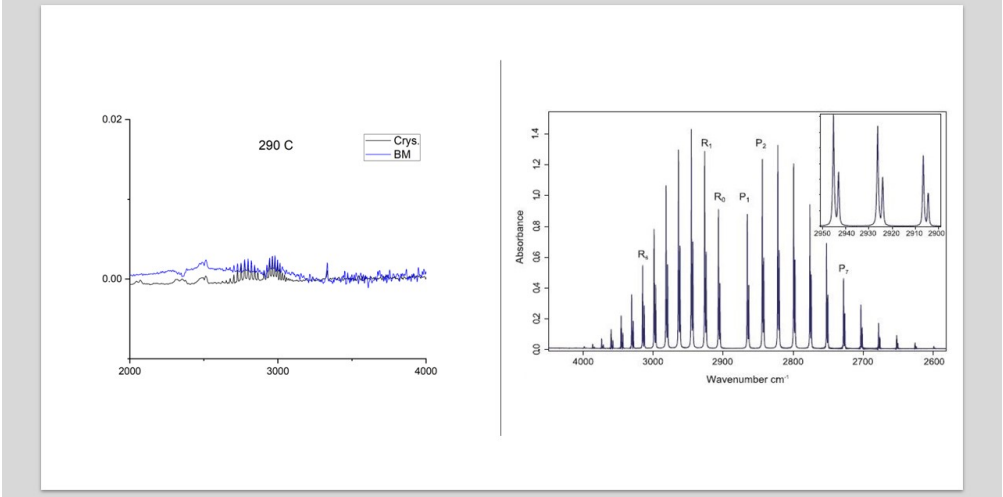

(a)

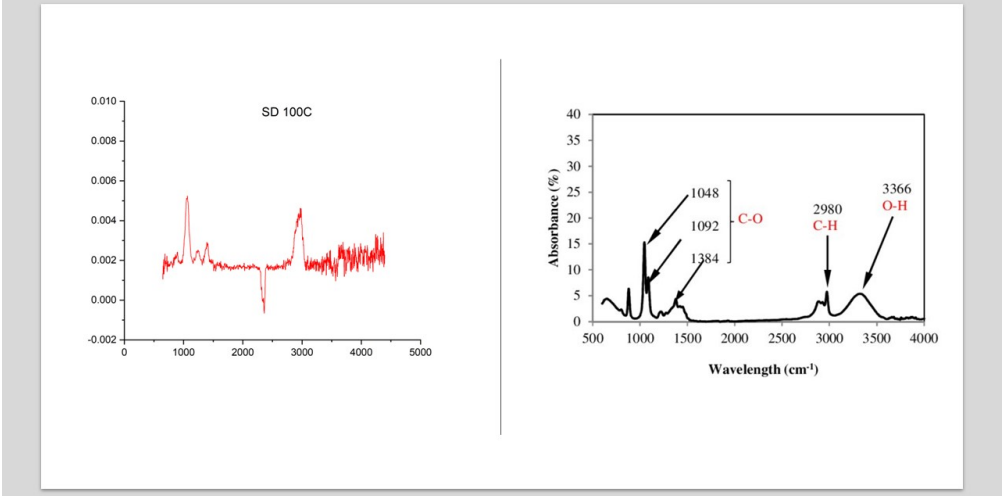

(b)

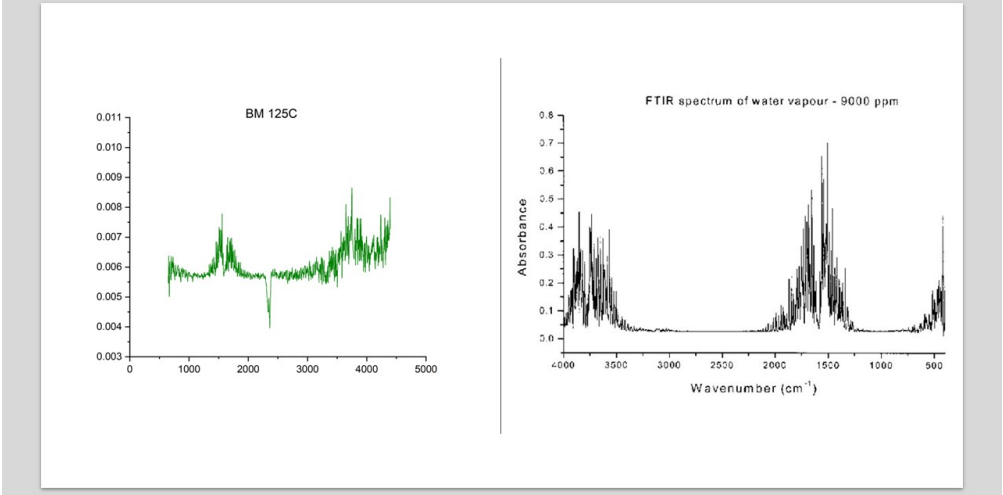

(c)

Figure 22: Comparisons between the (a)crystalline and quench cool IRs and HCL spectra, (b)spray dry and ethanol spectrum, and (c)ball mill and water spectrum respectively.

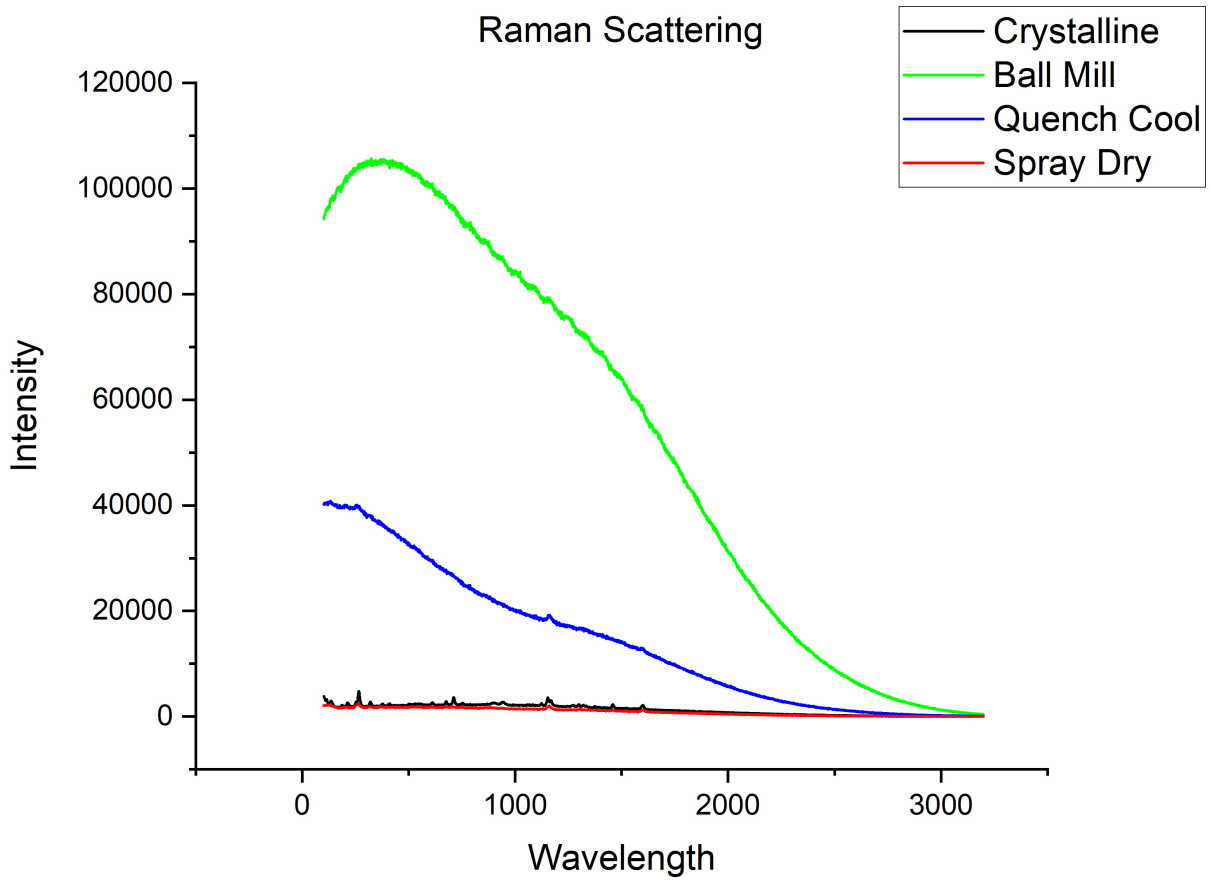

Figure 23: Raman Spectroscopy of all forms of our HCT sample. Quench cool and ball milled samples show at least some degree of flourescence while the spray dried and crystalline samples do not.

	Sample available for experiment?				
	DSC	TGA	FTIR	Raman	XRPD
Sample 1	Yes	No	No	No	No
Sample 2	Yes	Yes	Yes	Yes	Yes
Sample 3	Yes	Yes	No	Yes	Yes
Sample 4	Yes	Yes	Yes	Yes	Yes

Table 7: Doectaxel Experimental Parameters

	DSC 1	DSC 2	TGA
Initial Temperature	25 C	28 C	28 C
Isotherm?	No	Yes	No
Heating Rate	10 K/min	5 K/min	2.5, 5, 7.5, 10 K/min
Peak Temperature	192 C	160 C	250 C
Cooling Rate	10 K/min	2 K/min	10 K/min
Final Temperature	25 C	28 C	28 C
With Correction(s)?	Yes	No	Yes
Special Notes	none	This sequence of steps repeats five times in a row in one measurement	none

5.1.3 Experimental Methods

Differential Scanning Calorimetry (DSC) For our DSC measurements, we used sample sizes between approx. 3.5 to 4.0 mg, with one outlier sample having a 1.8 mg mass due to running out of that particular sample. Objective of the first tests were to determine reproducibility within the sample and see if the samples were polymorphic. Second test was largely an experiment to test a concept.

Thermogravimetric Analysis (TGA) and Fourier-Transform Infrared Spectroscope (FTIR) Our TGA-FTIR measurements acted to also confirm polymorphism, and utilized samples that had varying masses but volumetrically took up about half of the crucible.

Raman Microscope Raman data collection was supervised by Hery Mitsutake and used both the 532nm and 785nm lasers. Selected power for each test was one level below flourescence inducing power, and measurements were taken as snapshots. In our measurements, we wanted to see both the differences between the samples, and also compare to possibly degraded samples, and samples we knew weren't degraded but had been melted.

X-ray Powder Diffraction (XRPD) For our Docetaxel samples we outsourced the data collection to Nicolas Pierre Louis Magnard of the UCPH Department of Chemistry. He used a Brucker D8 diffractometer with a Cu K(alpha)1 radiation source in reflection mode. According to an email correspondance between myself and Nicolas, the Brucker D8 "works in a Bragg-Brentano geometry with - configuration, i.e. the sample is fixed and the X-ray source and detector are rotating."[17] Samples were placed on a zero-background silicon crystal sample holder. Data was collected on a 2Theta range of 5-70 degrees. In this segment of our study our goal was to use the XRPD data to determine the existence of polymorphs between our samples.

5.2 Results

5.2.1 Differential Scanning Calorimetry (DSC)

There are a few things we are able to deduce from our DSC results. 1. As seen in table 8), a sample is just as likely as not to be irreproducible.

2. Figure 24 shows samples 1 and 2 behaved similarly to each other, but very differently from samples 3 and 4 which were both unique in their pattern. This means that there are some form of bond differences between samples.

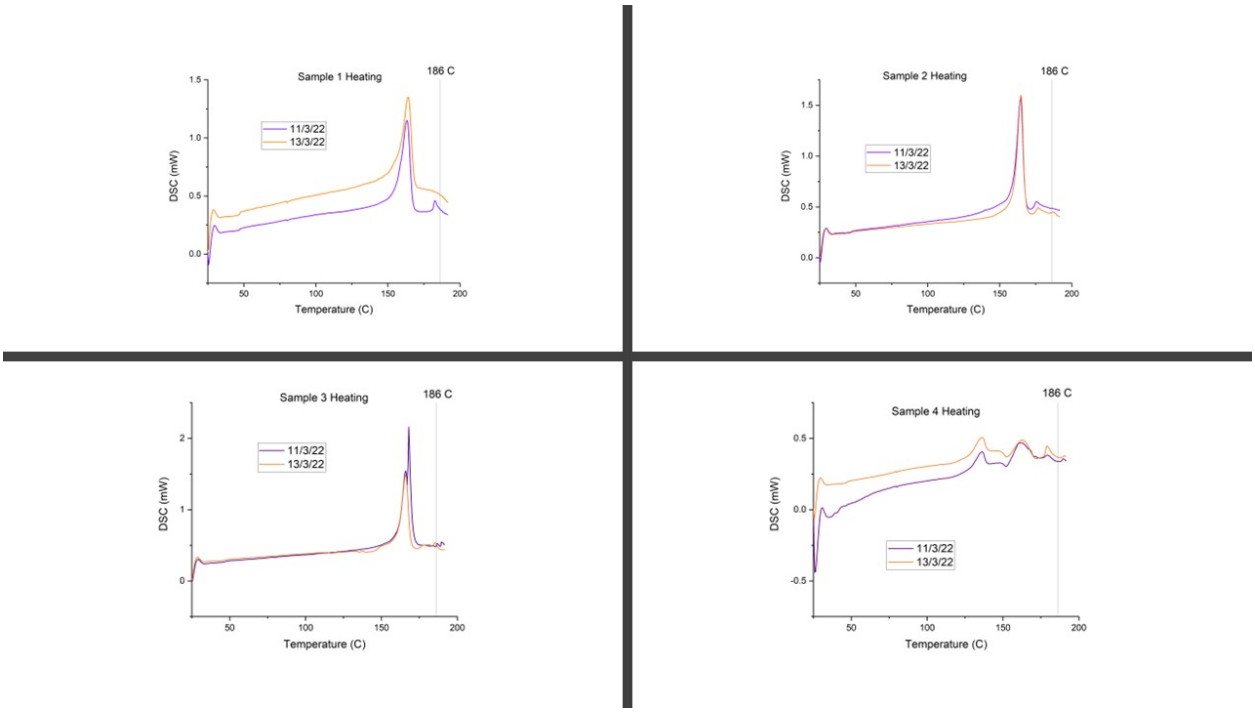

Figure 24: DSC results for samples 1-4 measured on two separate occasions, with dates of measurements labeled in the plots. All samples except for sample 4 (fig. 24(d)) show a prominent peak around the melting point. Samples 1 and 3 (fig. 24(a) and 24(c)) show irreproducibility before the earliest decomposition point, 186°C.)

Table 8: DSC Reproducibility

	Before decomp.	After decomp.
Sample 1	No	No
Sample 2	Yes	No
Sample 3	No	No
Sample 4	Yes	Yes

3. The likely reason for greater irreproducibility beyond 186 C is that DTX begins decomposing between 186-192 C, so the samples from the same batch measured on different days probably begin decomposing at different temperatures (fig. 24). This would require further testing to confirm.

During our oscillation test (fig. 25, we observed a melt in our first heating round, and then a series of what looks like glass transitions shifting from higher to lower temperatures with each successive heating round. The cooling phases begin jagged but after a few cycles flatten out, only to spawn new peaks at different temperatures on the fifth cooling cycle. This may be indicative of a restructuring of the crystal form or polymorphisation.

It is also possible that these peaks don't actually mean anything. Further testing is needed.

5.2.2 Thermogravimetric Analysis and IR Spectra (TGA-FTIR)

The most important results we are able to discern from our TGA data (figs. 27 - 29) is that all samples lose about the same amount of mass by the end of the heating phase, with each sample having lost between 40-45% at 250 °C (depending on heating rate). This will be important when we look at the FTIR data (table 5.2.2 and figures 30-32).

As we can see from the TGA (figs. 27 - 29), there are clear differences between the degradation over increasing temperature for all samples. From our corresponding results though, we confirm that all samples

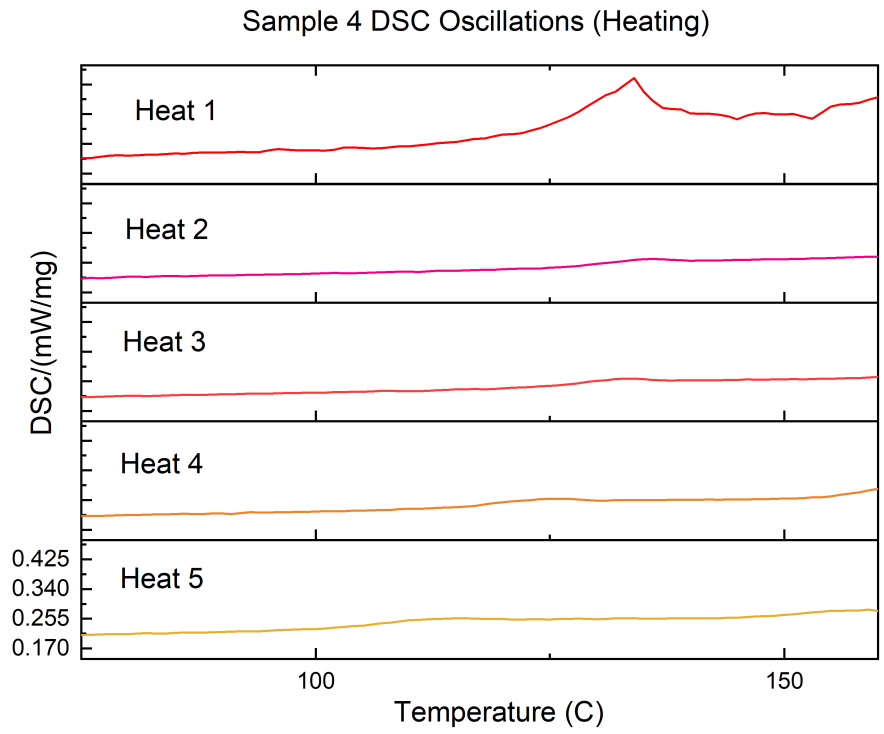

(a)

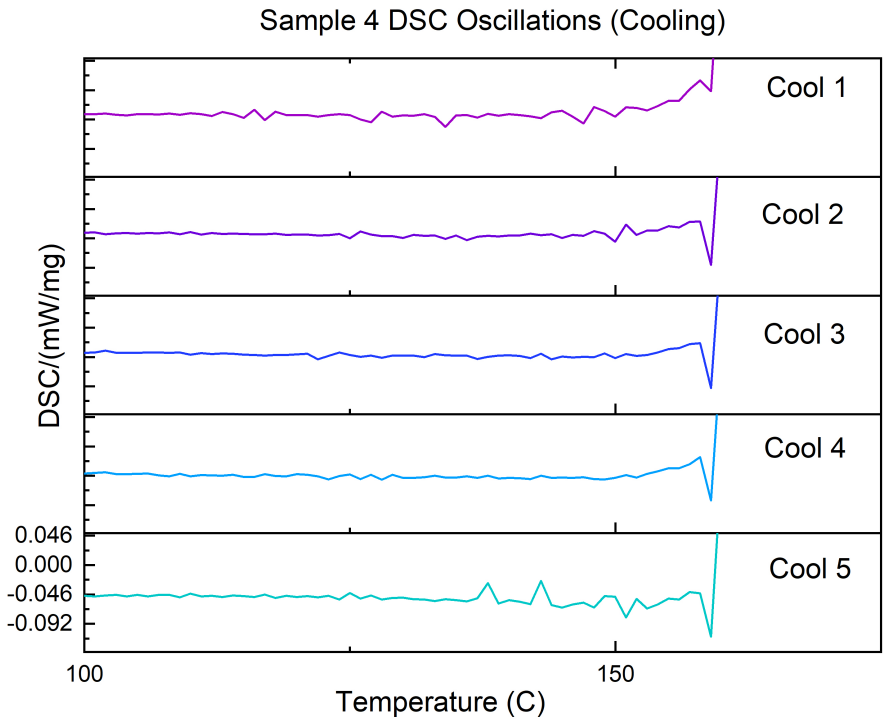

(b)

Figure 25: Oscillating DSC experiment results. We can observe notable differences between each cycle. (Top, 25(a)) Heating cycle 1 shows a sharp melting peak around 130 °C, while heating cycles 2-5 are much more relaxed, showing glass transitions that occur at decreasing temperatures as the cycles repeat. (Bottom, 25(b)) Cooling cycles 1-4 show steadily decreasing activity along the cycle progression, but then cooling cycle 5 shows a marked jump in activity.

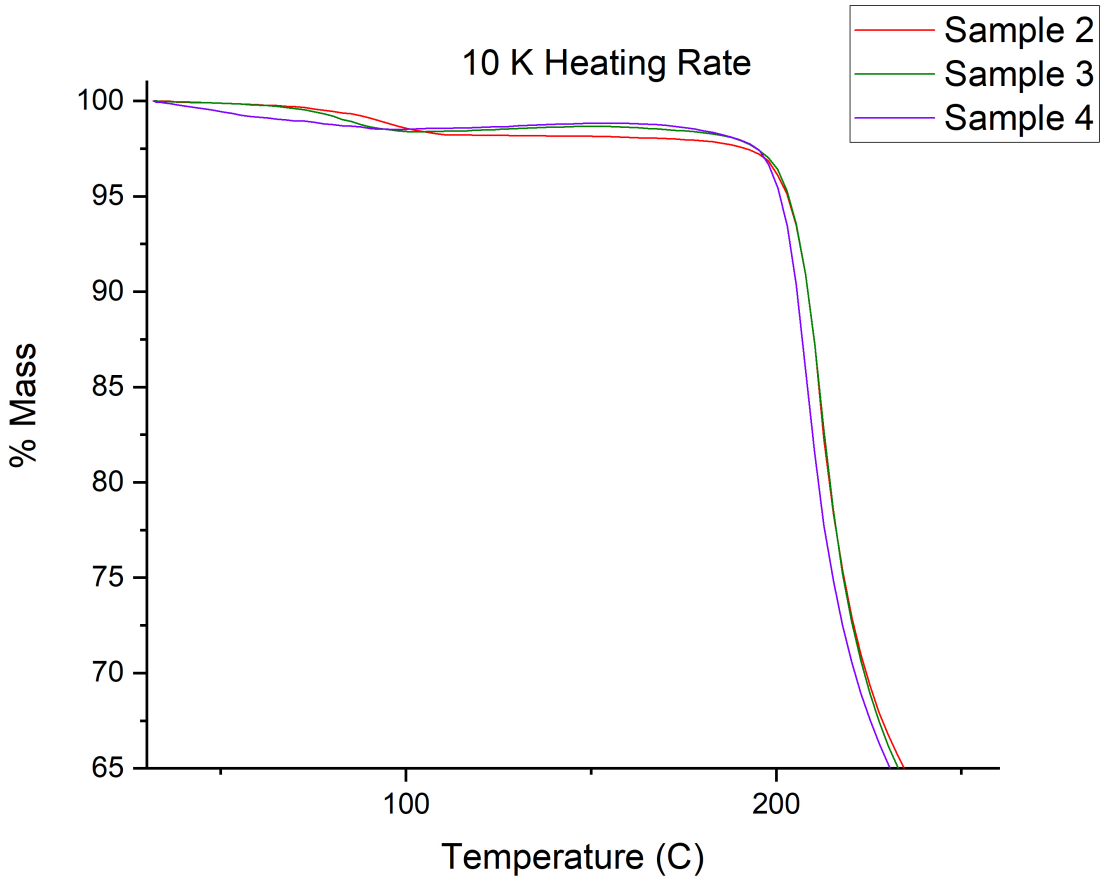

Figure 26: TGA comparison of samples 2-4 at the same heating rate (10 K/min).

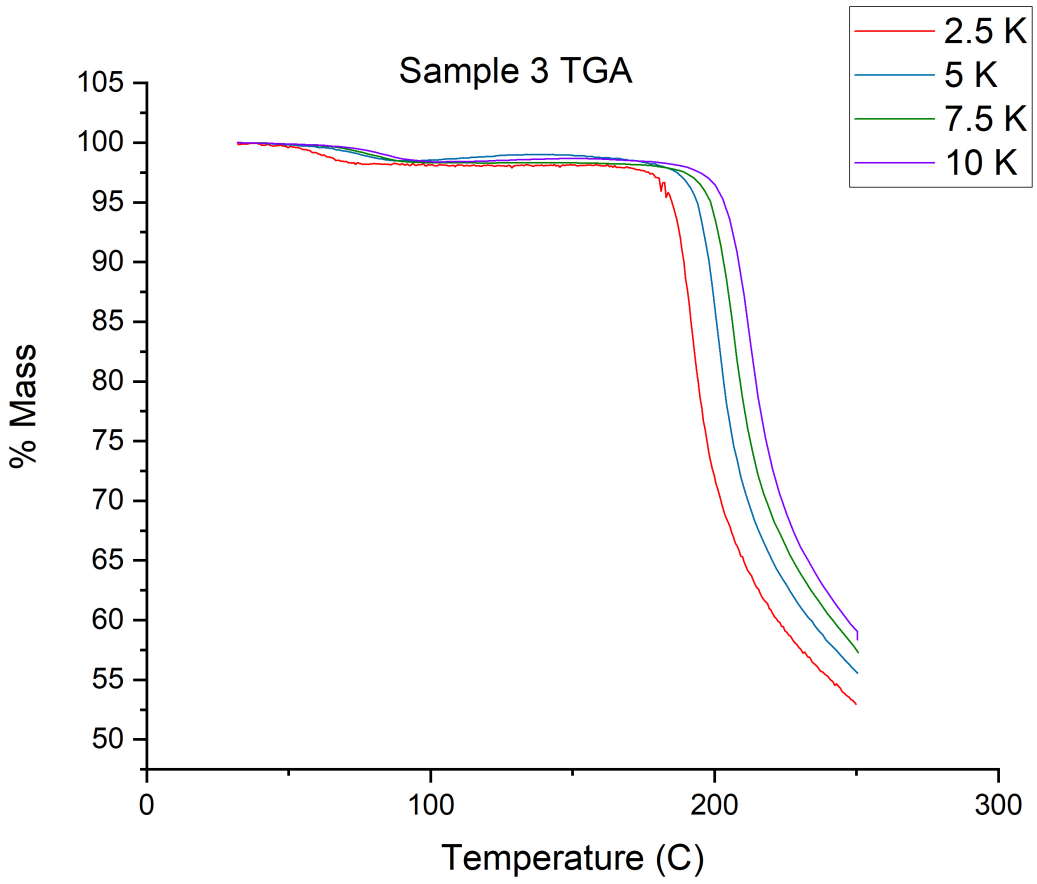

Figure 27: Comparison of mass loss over temperature at heating rates of 2.5K/min, 5 K/min, 7.5 K/min, and 10 K/min for sample 3.

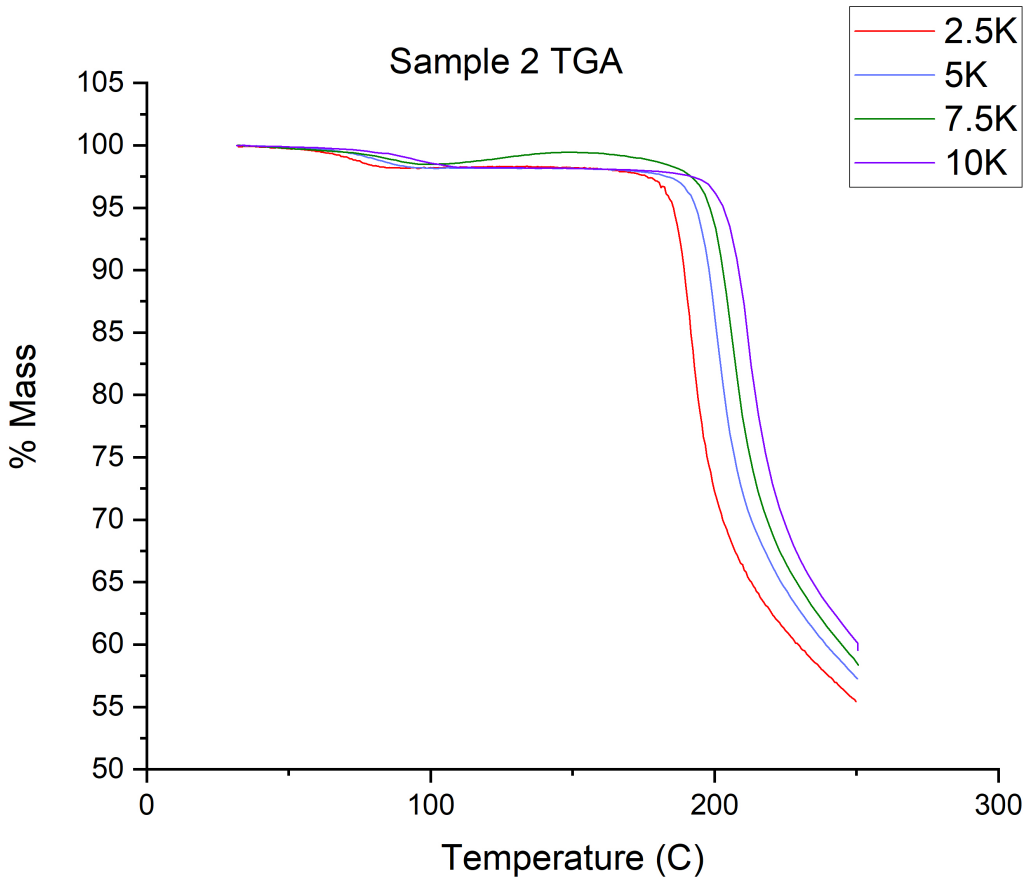

Figure 28: Comparison of mass loss over temperature at heating rates of 2.5K/min, 5 K/min, 7.5 K/min, and 10 K/min for sample 2.

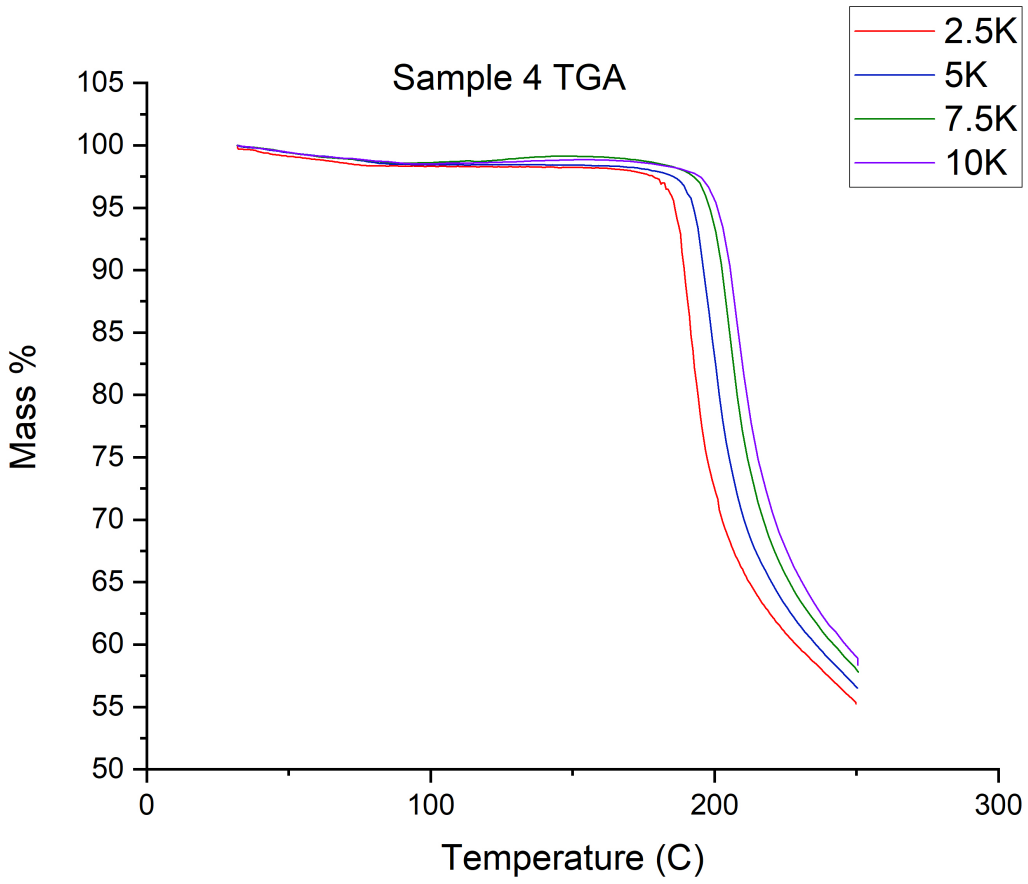

Figure 29: Comparison of mass loss over temperature at heating rates of 2.5K/min, 5 K/min, 7.5 K/min, and 10 K/min for sample 4.

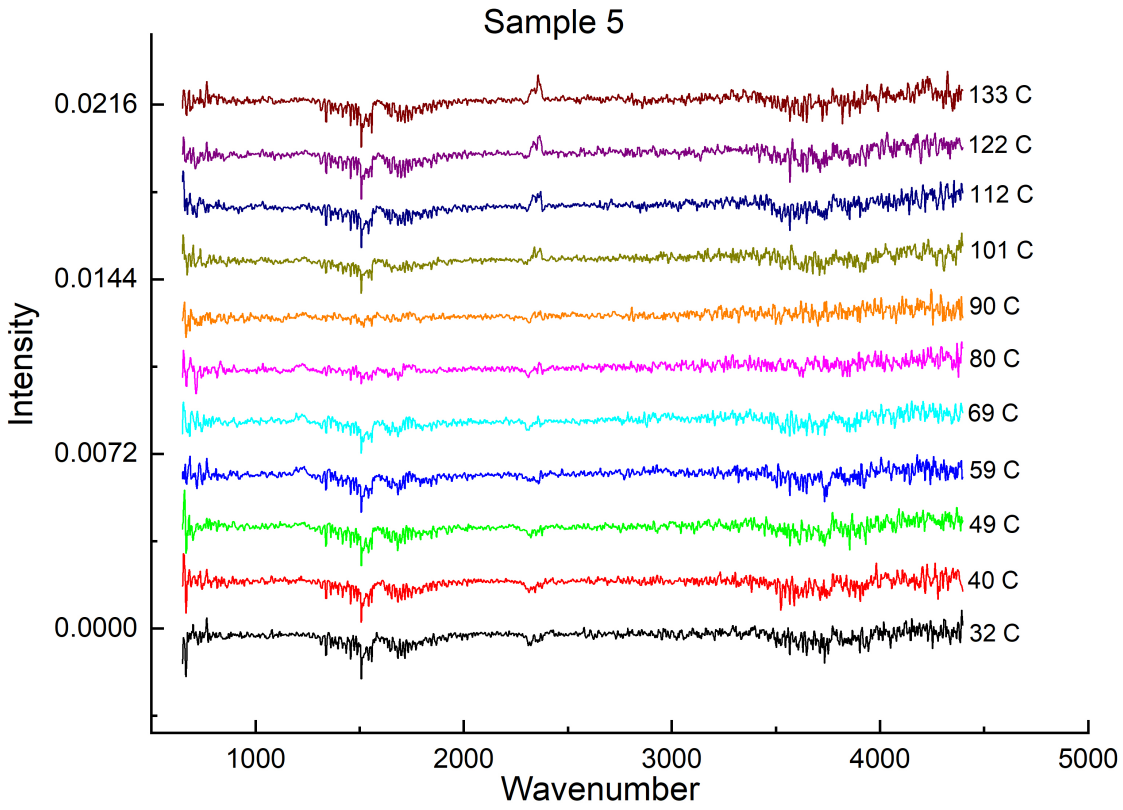

(a)

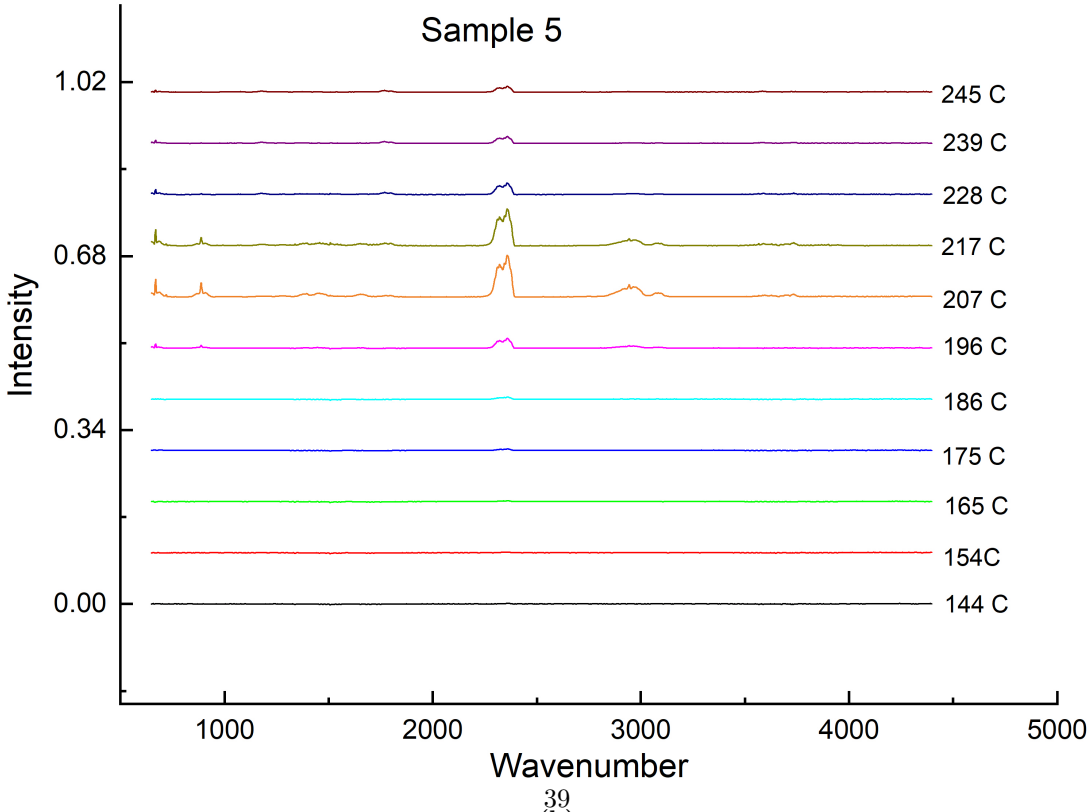

(b)

Figure 30: IR spectroscopy at relevant temperatures for sample 5.

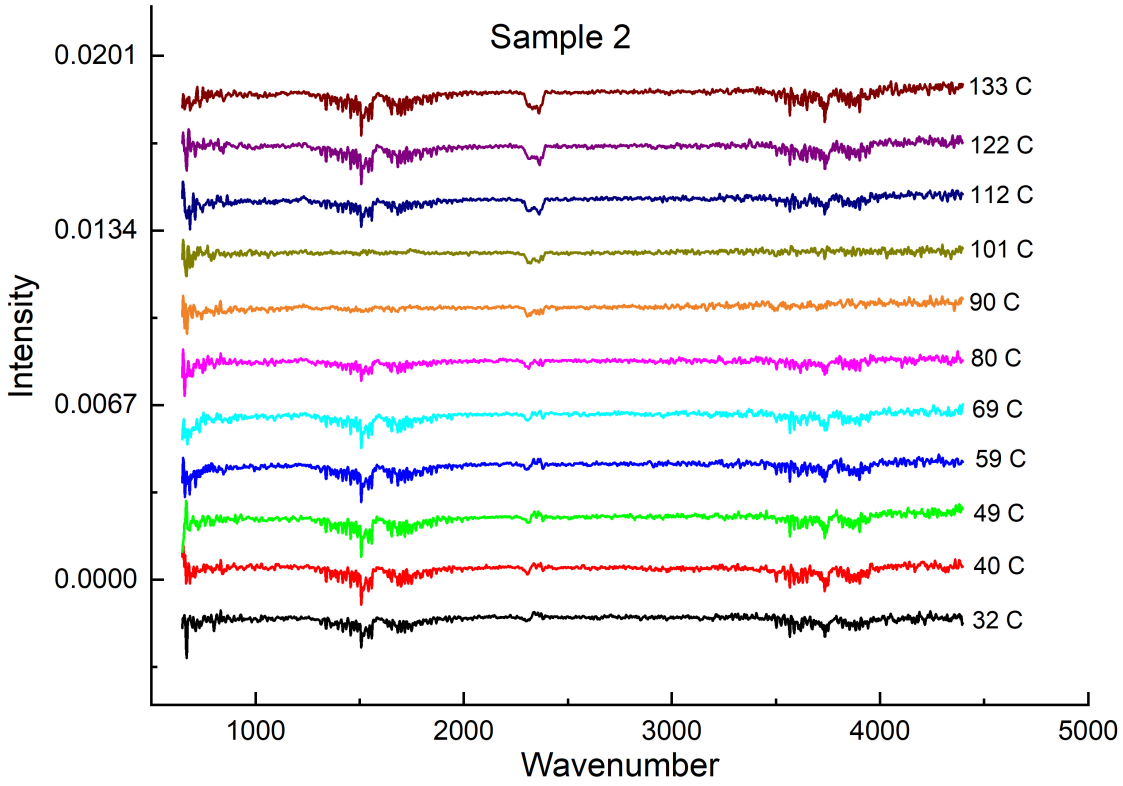

(a)

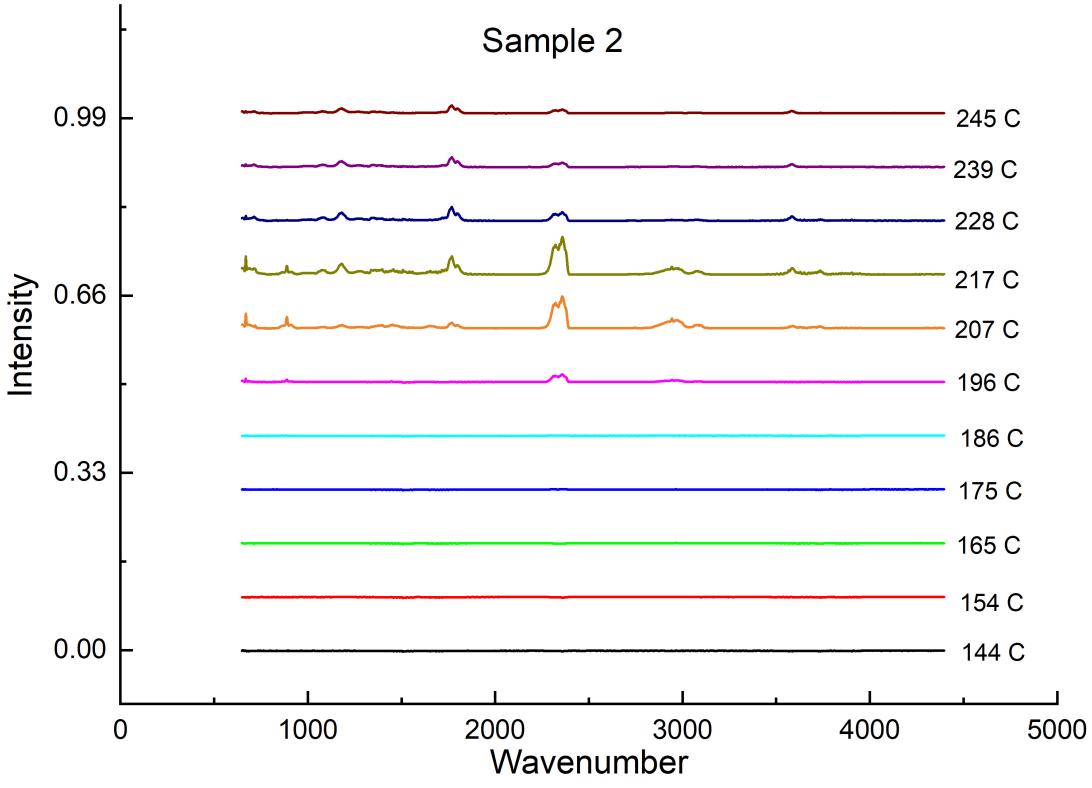

(b)

Figure 31: IR spectroscopy at relevant temperatures for sample 2.

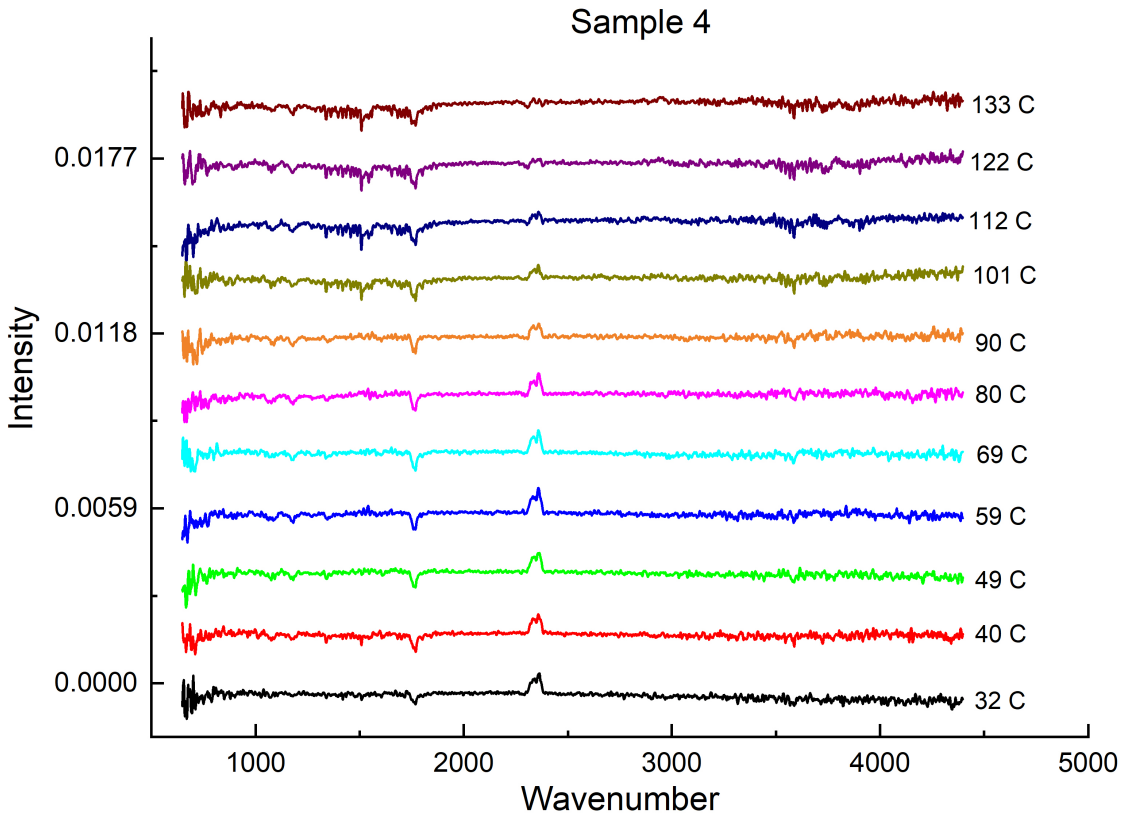

(a)

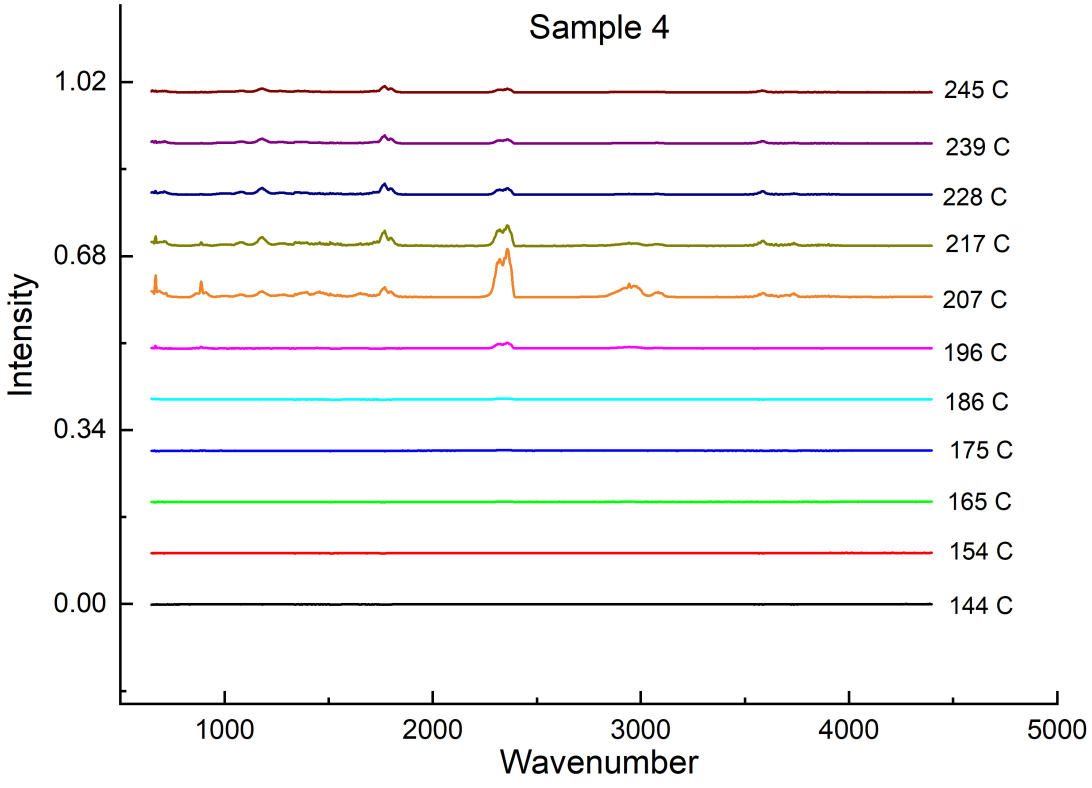

(b)

Figure 32: IR spectroscopy at relevant temperatures for sample 4.

lose approximately the same amount of mass over temperature. This would imply that there is a difference between the strength of certain bonds between samples. So some compounds are more likely to be shuffled off than others comparatively between the samples. Something interesting seen comparing samples 5 and 2 (the same sample measured 1-2 years apart) from figures 30 and 31, is that sample 5 emits much more before the decomposition point than sample 2, which loses its mass almost solely due to decomposition. My hypothesis on this is that as the sample ages over time, it settles into a "relaxed", more thermodynamically stable state, possibly a polymorph. It can also be figured that there is some sort of solvent being emitted by sample 4 (fig. 32). As it relates to the DSC data I would hypothesize that the reproducibility of sample 2's DSC measurement (fig. 24) can be observed by the flatness of the spectral measurement for sample 2 (fig. 31) around 186 °C. This would require more testing on both counts to confirm.

Temperature (C)	Sample 5	Sample 2	Sample 4
32	Ethanol	Minor CO2	CO2
40	Ethanol	Minor CO2	CO2
49	Ethanol	Minor CO2	CO2, **Something(1050-1200)
59	Ethanol, **Something(1200-1300)	Minor CO2	CO2, **Something(1050-1200)
69	Ethanol, **Something(1200-1300)	Minor CO2	CO2, **Something(1050-1200)
80	CO2, **Something(1200-1300)	——	CO2, **Something(1050-1200)
90	CO2, **Something(1200-1300)	——	CO2, **Something(1050-1200)
101	Ethanol, CO2	——	Minor CO2, **Something(1050-1200)
112	Ethanol, CO2	——	Minor CO2, **Something(1050-1200)
122	Ethanol, CO2	——	Minor CO2, **Something(1050-1200)
133	Ethanol, CO2	——	**Something(3000)
144	——	——	——
154	Minor CO2	——	——
165	——	——	——
175	Minor CO2	——	——
186	Minor CO2	——	——
196	Decomposition*	Decomposition*	Decomposition*
207	Decomposition* decomposition peak @ 211	Decomposition*	Decomposition* decomposition peak
217	Decomposition* decomposition peak @ 211	Decomposition* decomposition peak	Decomposition*
228	Decomposition*	Decomposition*	Decomposition*
239	Decomposition*	Decomposition*	Decomposition*
245	Decomposition*	Decomposition*	Decomposition*

*CH=CH-C=CH2; double group(s): CH3 and CH2; C=O conjugated; O=C=O; N-H; C-H; free OH stretching vibrations [5]

5.2.3 dTGA and the Kissinger Model

For samples 2 and 3, we had to disqualify the thermograms from the 7.5K and 5K heating rates respectively, because the TGA showed a mass gain at some point (indicated by an upward bump on the plot in figures 28 and 27), so those Kissinger models will be using three points. Sample 4 had all four rates usable (figure 29). Origin 2020 was used for data treatment. A Gaussian fit using the NLFit was employed to determine the peaks that naturally occurred. All three samples showed only one peak for each heating rate. Through the data given with the fit I found the following (tables 9, 12, and 11): [5]

Next I manually annotated each peak location using "find peak" under "analysis" on the software. There resulted some small discrepancies between the Origin given point and the manually found point, but I believe them to be negligible.

We can see the difference between activation energies for samples 2 and 5, which are the same sample measured

Table 9

Sample 2

Rate	Td1
2.5K	191.94506 +- 0.19256
5K	202.61922 +- 0.27867
7.5K	n/a
10K	213.62501 +-0.41528

Sample 3

Rate	Td1
2.5K	193.81622 +- 0.37279
5K	n/a
7.5K	207.96658 +- 0.27813
10K	214.04368 +-0.14556

Sample 4

Rate	Td1
2.5K	193.31725 +- 0.19303
5K	200.06054 +- 0.27778
7.5K	207.19167 +- 0.42199
10K	211.07002 +-0.49322

Table 10: Calculated slopes for each sample based on figures 33-35

	Slope
Sample 2	-0.39182 +- 0.13778
Sample 3	-0.53088 +- 0.02192
Sample 4	-0.46511 +- 0.04435

Table 11: Calculated activation energy for samples 2-5

Sample	Activation energy kJ/mol
2	101.7135
3	113.8436
4	123.9368
5	107.37

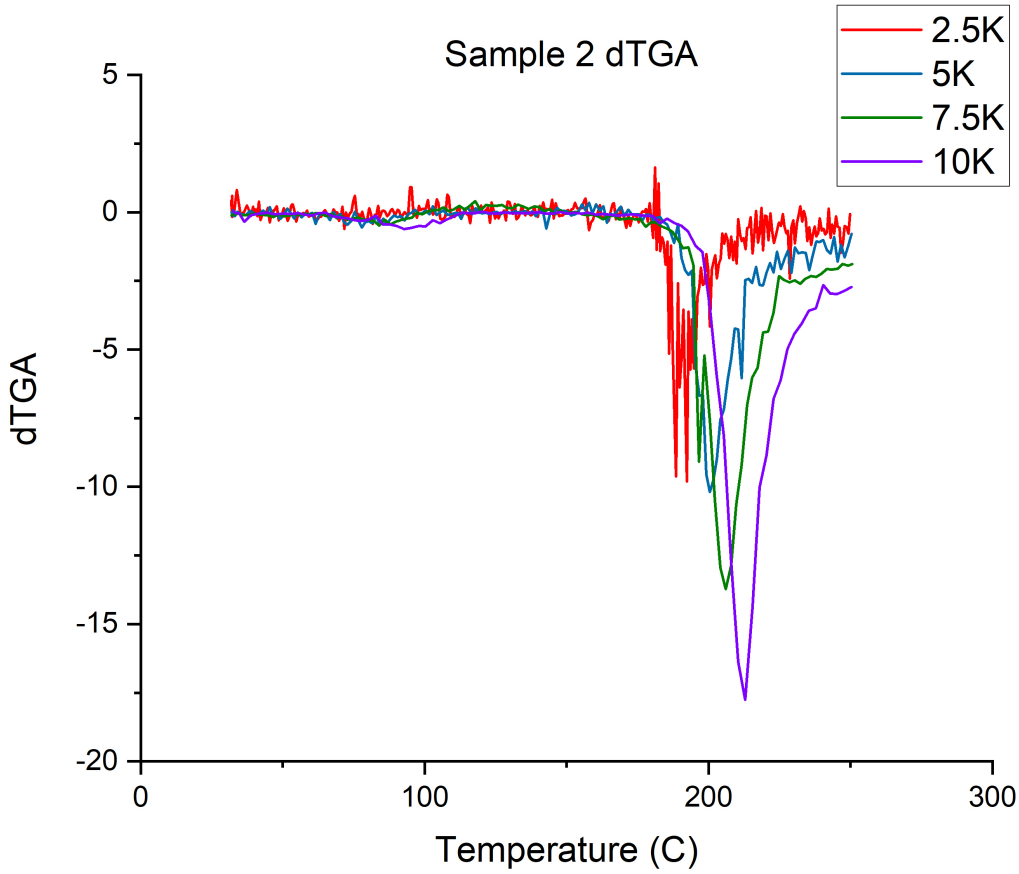
Sample 2 dTGA
2.5K
5K
7.5K
10K
dTGA
Temperature (C)
5
0
-5
-10
-15
-20
0
100
200
300

(a)

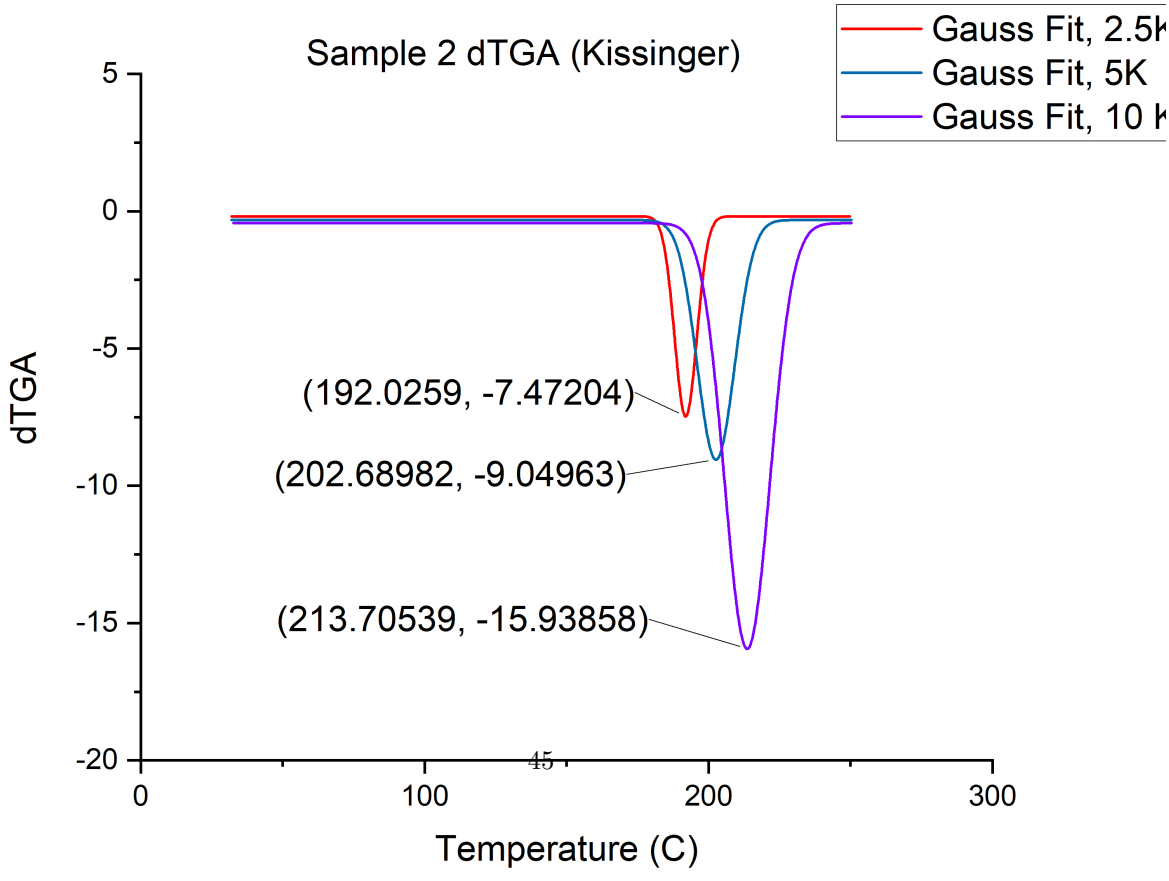
Sample 2 dTGA (Kissinger)
Gauss Fit, 2.5K
Gauss Fit, 5K
Gauss Fit, 10 K
(192.0259, -7.47204)
(202.68982, -9.04963)
(213.70539, -15.93858)
dTGA
Temperature (C)
5
0
-5
-10
-15
-20
0
100
200
300

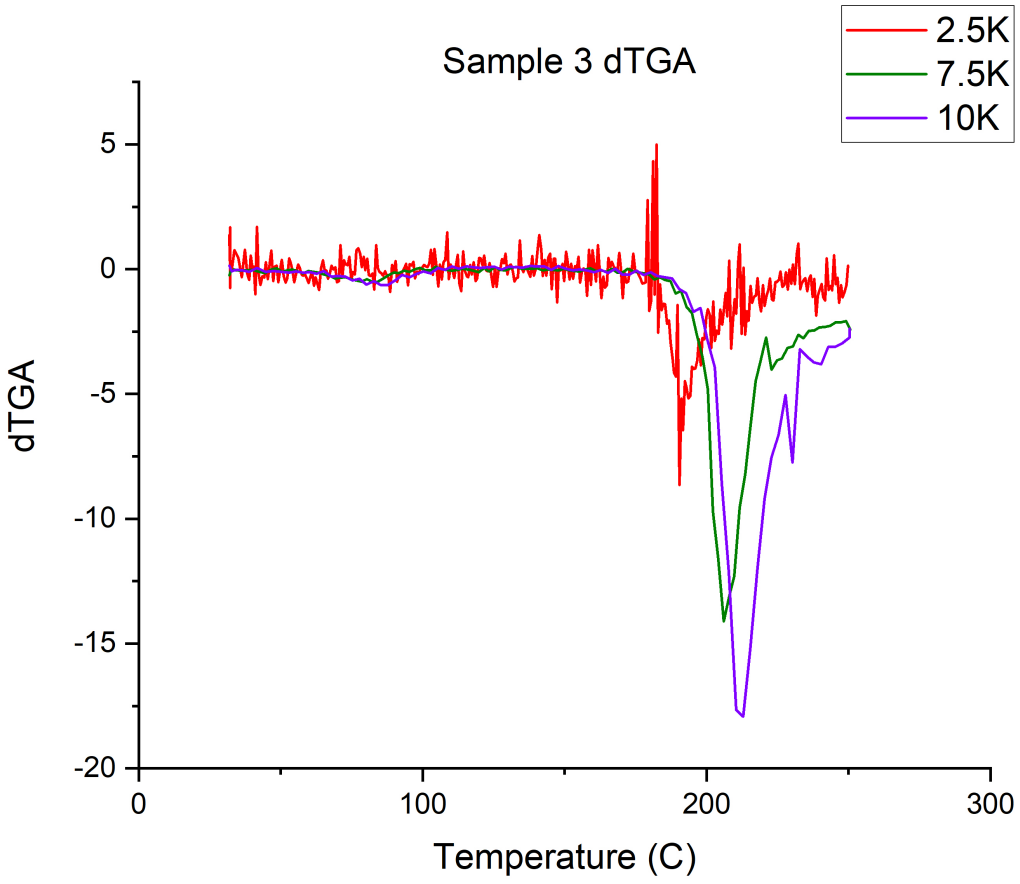
Sample 3 dTGA
2.5K
7.5K
10K
dTGA
Temperature (C)
5
0
-5
-10
-15
-20
0
100
200
300

(a)

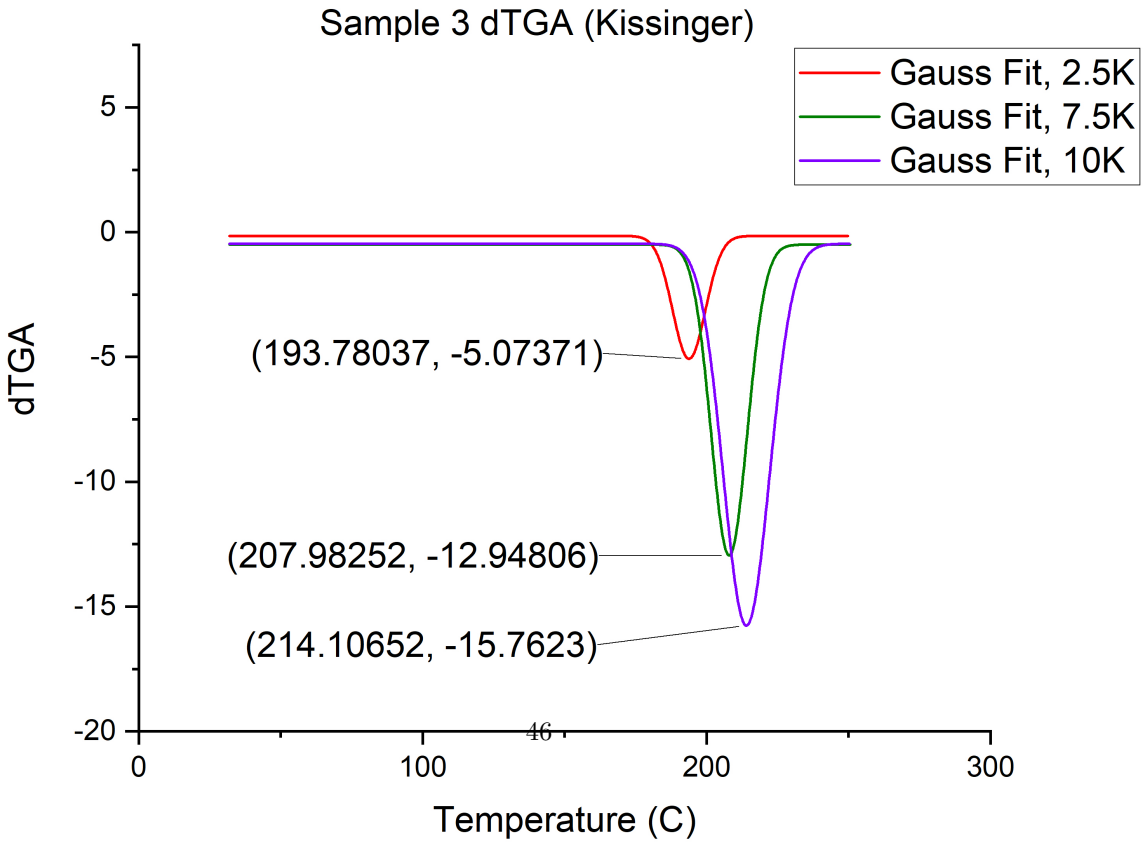
Sample 3 dTGA (Kissinger)
Gauss Fit, 2.5K
Gauss Fit, 7.5K
Gauss Fit, 10K
(193.78037, -5.07371)
(207.98252, -12.94806)
(214.10652, -15.7623)
dTGA
Temperature (C)
5
0
-5
-10
-15
-20
0
100
200
300

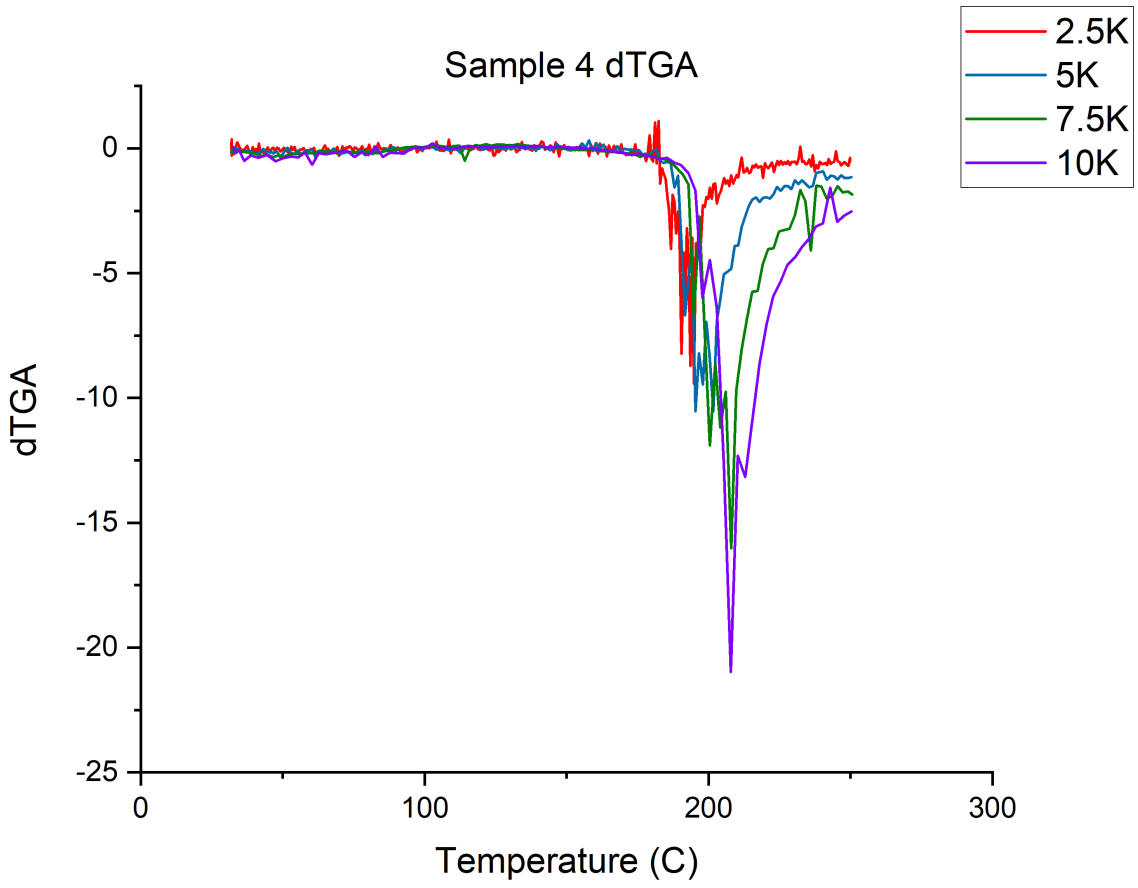
Sample 4 dTGA
2.5K
5K
7.5K
10K
dTGA
0
-5
-10
-15
-20
-25
0
100
200
300
Temperature (C)

(a)

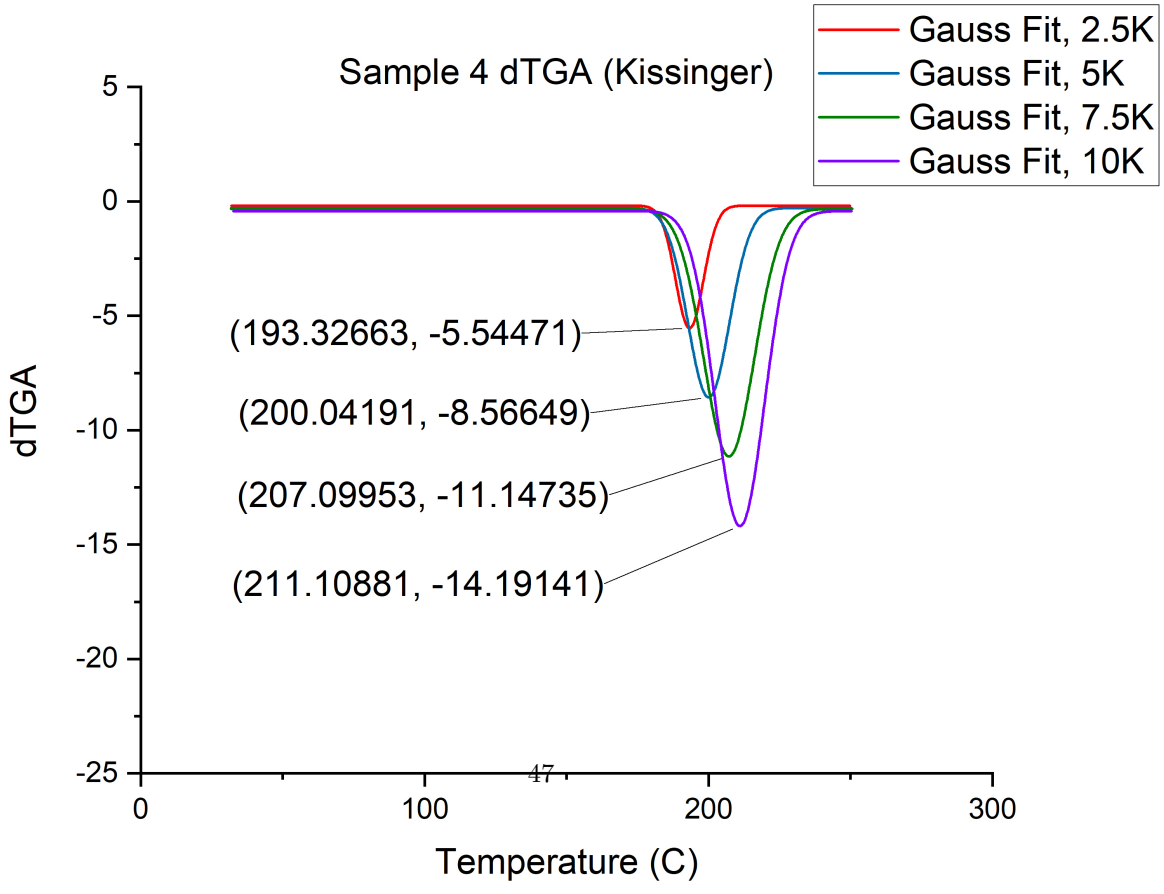
Sample 4 dTGA (Kissinger)
Gauss Fit, 2.5K
Gauss Fit, 5K
Gauss Fit, 7.5K
Gauss Fit, 10K
(193.32663, -5.54471)
(200.04191, -8.56649)
(207.09953, -11.14735)
(211.10881, -14.19141)
dTGA
5
0
-5
-10
-15
-20
-25
0
100
200
300
Temperature (C)

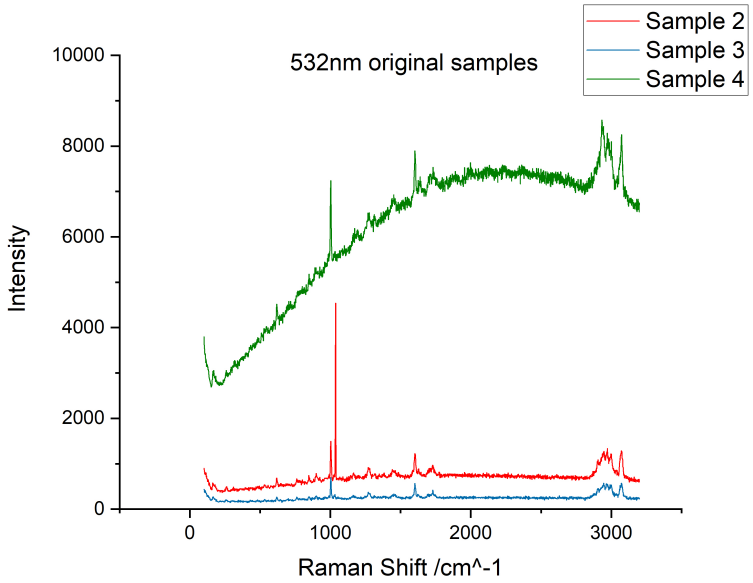

Figure 36: Uncooked samples measured at 532mn. Sample 4 shows some fluorescence but differences in the raman shifts and intensities are still easily observable between samples.

over a year apart, in 2022 and 2020 respectively. Sample 2's activation energy is noticeably lower than sample 5's. I'm lead to hypothesise that the reason for this is the "rest" that sample 5 underwent between 2020 and 2022 allowed the bonds of the DTX to relax as they settled into a more thermodynamically stable state. This can be further supported by the activation energy of sample 4 which is the highest. We are aware that there is some solvent that came with sample 4, and an addition of solvent makes any drug less stable thermodynamically.

5.2.4 Raman Scattering

Our Raman microscope results (figs. 36 and 37) for the uncooked samples are showing that there are differences between samples in both intensity and raman shift.

When we use the 532 nm laser, we see a peak in sample 2's reading where we don't see peaks for the other samples at 1038 cm^-1, and a peak unique to sample 4 at about 1633 cm^-1 (fig 36). This same laser readout shows us that other than the sample 2 specific peak near 1000 cm^-1, sample 4 has much greater overall intensity wherever there are peaks (especially around 1500 and 3000 cm^-1).

The 785nm laser shows differences in intensities between samples at various peaks as well, but the more interesting observations stemming from the unique peaks (or lack thereof) seen throughout the measurement (fig. 37). The most readily observable wavenumbers where there are differences in peak occurrence are as follows:

450, 500, 550, 700, 800, 950, 1050, 1200, 1350, 1500, 1650, 1750, and 2800-3200 cm^-1.

The most important piece of information gleaned from all measurements of the cooked samples is that once heated beyond a certain temperature, the sample shows fluorescence dependably within the Raman microscope (figs. 38-40). This occurs even before any decomposition takes place as seen by sample 4 after 160C DSC treatment. My initial hypothesis on this is that fluorescence occurs after transition from an opaque powder to a clearer, glass-like form through melting. In order to confirm this we would have to take measurements of samples heated to various temperatures and see where fluorescence starts.

Differences in Raman intensity between samples can mean that there is a difference in bond strength between the same bonds, with higher intensity indicating a stronger bond. This would mean that the bonds between the lattices in sample 2 are stronger than the other samples. The differences between the Raman shifts shows that these bonds are different lengths, orientations, or locations. This would make sense since we know sample 2 is a pure, untreated DTX powder, while sample 3 has some heat and x-ray treatment and sample 4 is thought to have some sort of solvent in the batch (this is unconfirmed). So, the bond strengths and locations/orientations/lengths should be different.

Also as a minor note, we can see that the results from our 785nm Raman measurements (fig. 37) confirm our FTIR measurements from the readings around 3000 cm^-1, and vice versa (figs. 30-32). So that's nice.

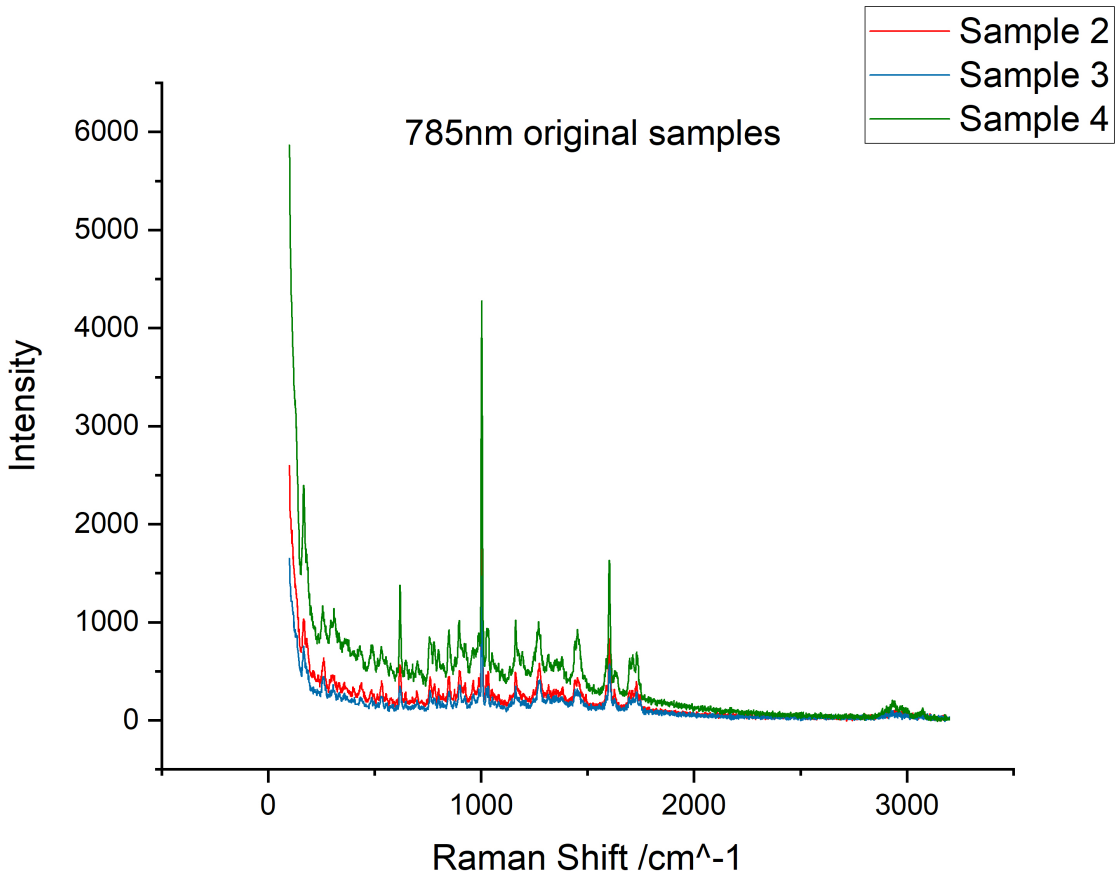

Figure 37: Uncooked samples measured at 785mn. No fluorescence is observed, and differences in peak locations and intensities among samples are very obvious.

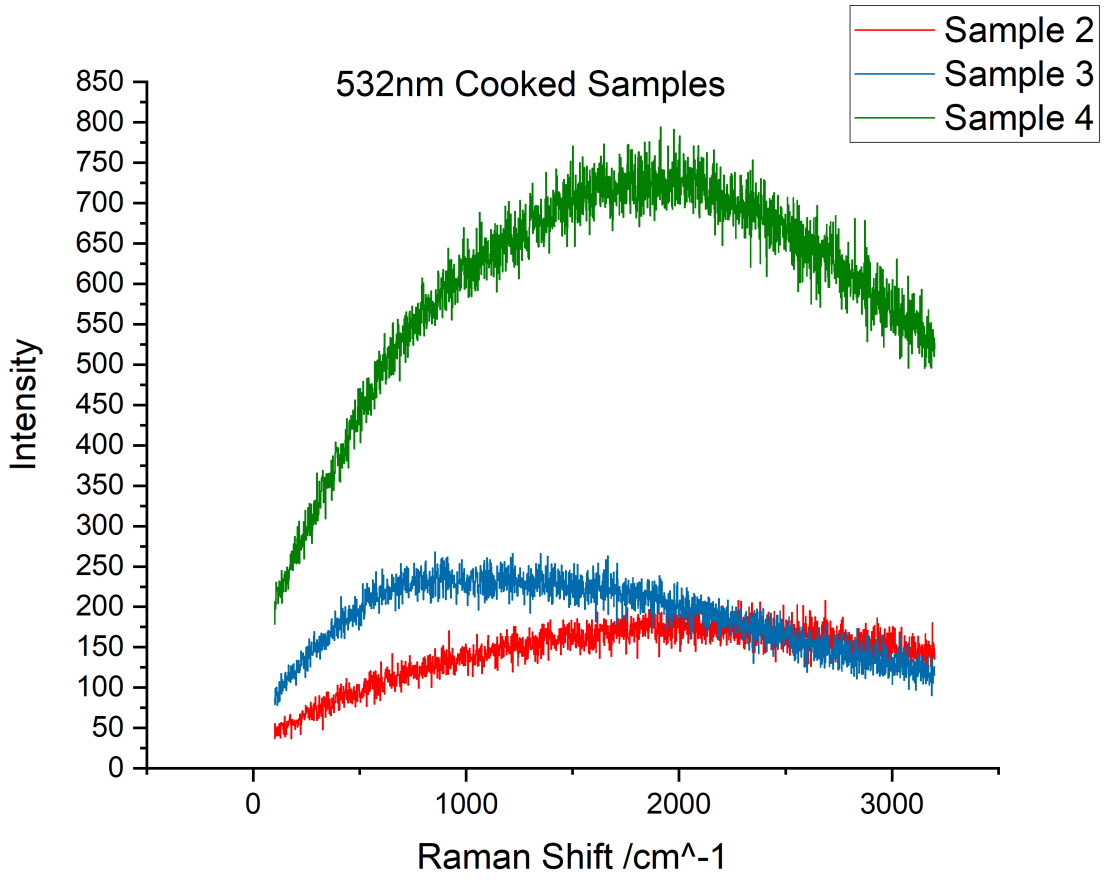

Figure 38: Cooked samples measured at 532mn.

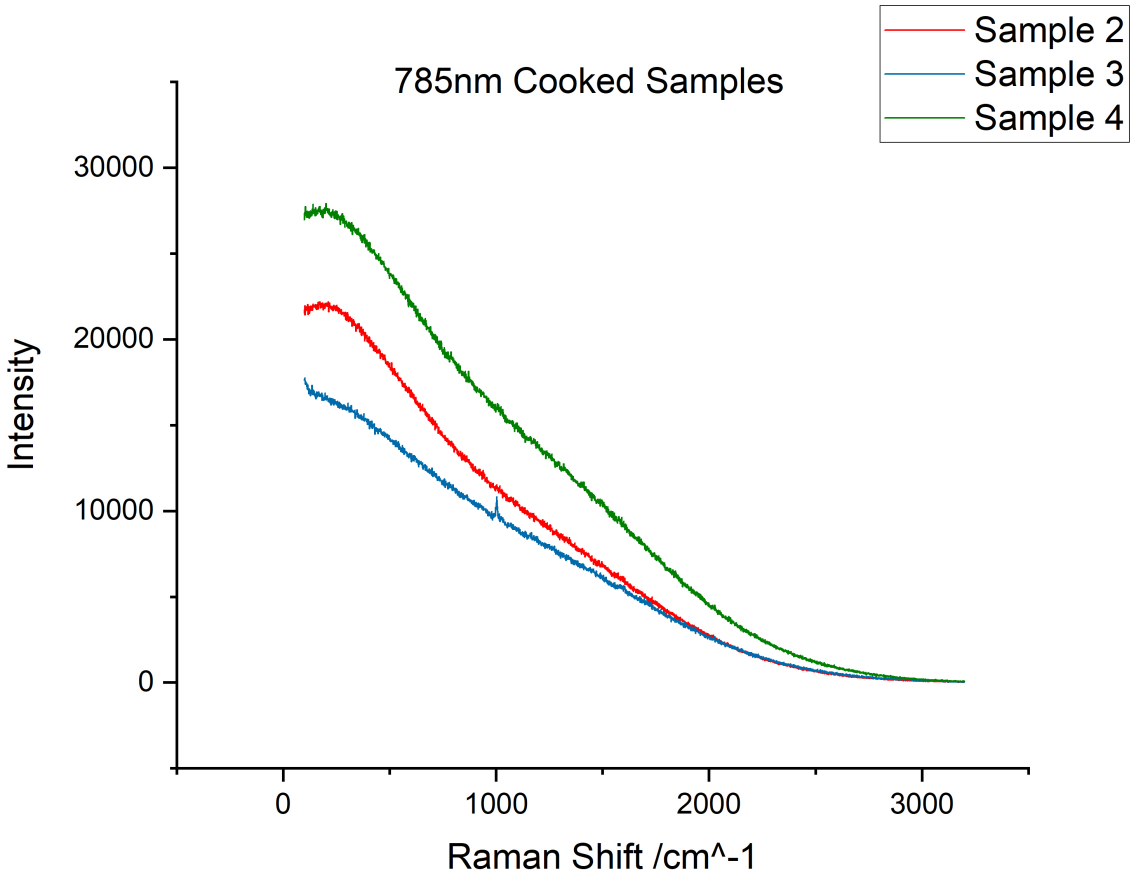

Figure 39: Cooked samples measured at 785mn.

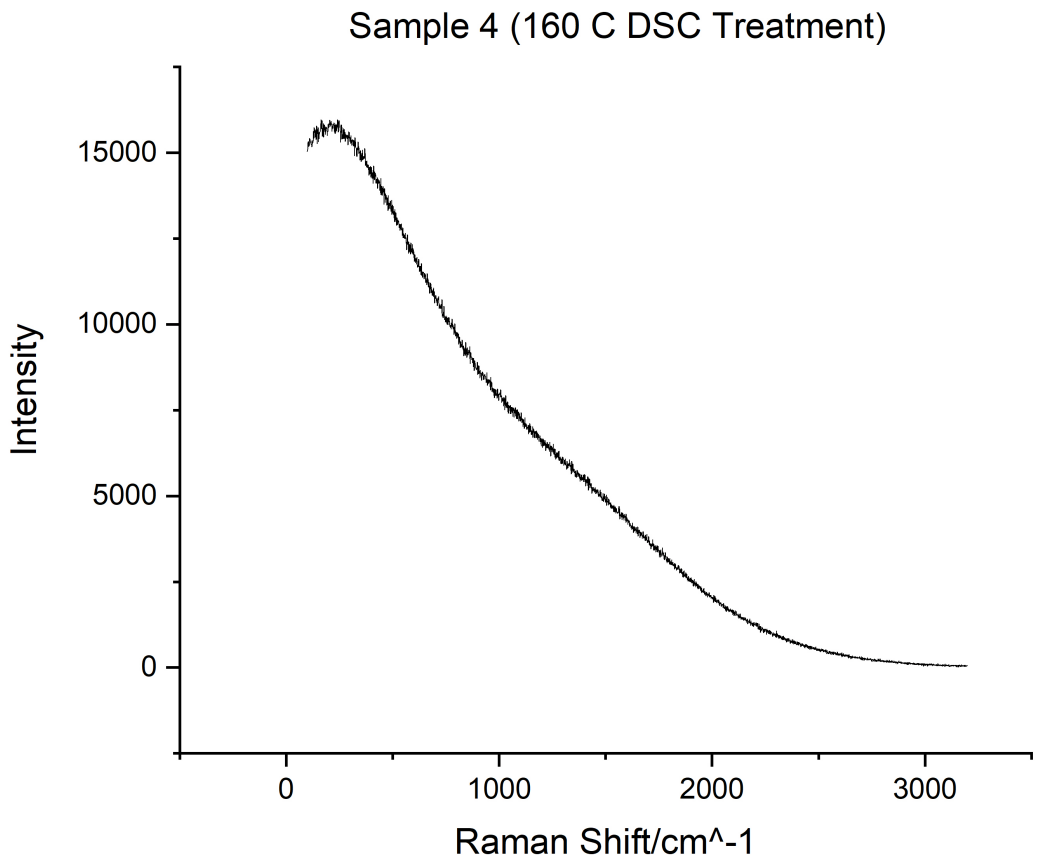

Figure 40: Raman measurement for a sample from the sample 4 batch that was treated up to 160 C.

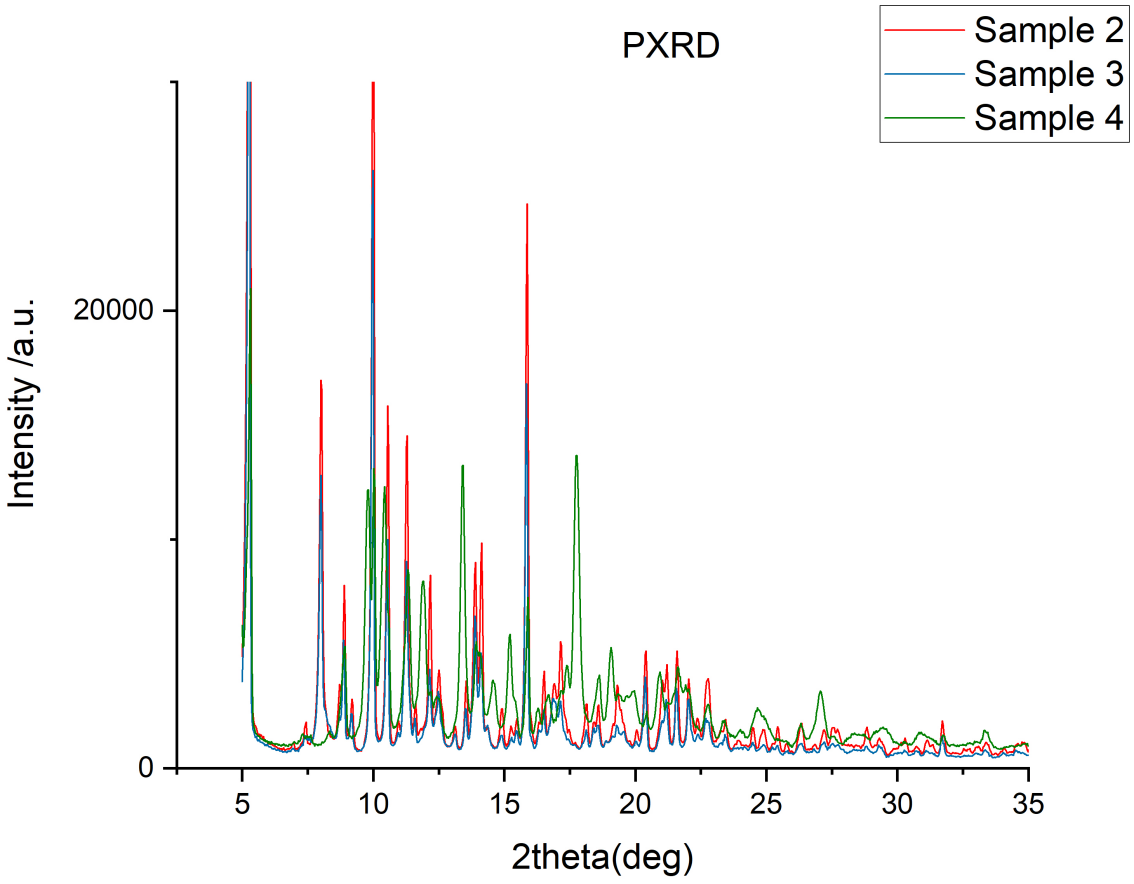

Figure 41: XRD of samples 2-4.

5.2.5 X-ray Powder Diffraction (XRPD)

Our XRPD results show a wealth of differences in peak locations between samples, as seen by figure 41, and each sample is unique in it's measurement. This confirms that there are different locations/orientations for the bonds, and therefore these three samples are definitive polymorphs of each other.

6 Chapter 6: Comparison of Results and Overall Conclusions

Our thermodynamic data is showing us clear differences in the local bonding of these different drug forms. The base molecule is the same across the board, and as we observed at the DESY synchrotron, there are no shifts in the bond distance probabilities between HCT forms. So the factors that influence the disparities we've observed in things like Tg and recrystallization points, as well as in the magnitudes of endothermic reaction and energy absorbed during melting, must be related to inter-molecular bonding.

Why does the spray dried form require so much less energy and heat to recrystallize than the ball milled samples, which are more reminiscent of the quench cooled HCT in terms of thermodynamic behavior? This despite the fact that both have impurities. The quench cooled HCT is our only purely produced amorphous form. My first hypothesis leads me to believe that this is because of the difference in impurities. The spray dried samples have residue from ethanol, which is an organic compound, while stainless steel is an inorganic metal. It would stand to reason that the organic HCT and the organic ethanol would more easily interact than organic HCT to inorganic steel. This more comfortable interaction may interfere with the bonds between these HCT molecules when they are in the fluid-mimicking amorphous form, eroding its stability. That being said, nothing can be proclaimed with confidence without observable data, and this is an avenue that would need exploring before claiming any facts. The next tests I would

recommend would be wide angle x-ray scattering, to see intensities at angstrom distances further than the lengths of the HCT molecule, and solid state NMR to combine with the small angle scattering data we already have.

Each form of HCT had differing TGA and IR results, this means that not only did they both decompose/oxidise differently despite being the same molecule, they also emit different compounds over time. The IR data shows us that the crystalline and quench cooled samples are very similar in their emissions, staying largely dormant until after the melting point, and emitting H-Cl, Sulfur Oxides, and Nitrogen Oxides upon decomposition (although the quench cool to a lesser degree for certain emissions and at slightly different temperatures). Quench cooled samples showed more noise, and there is a questionable pattern around 1000 1/cm between 50 °C and 150 °C, but I have not figured out what it is yet. Spray dried samples emit ethanol between 75 °C and 125 °C (not too surprising) [18], and while they will still emit most of the same compounds the crystalline and quench cooled forms do during decomposition, it is to a much lesser extent and little-to-no H-Cl comes out. In terms of H-Cl the same holds true for the ball mill samples as well, but unlike the spray dry, they emit no ethanol, and instead emit small amounts of water beyond 50 °C.[19] The emission of water by the ball mill form is slightly more head-scratching than spray dry's emission of ethanol, so further research is needed.

The question then becomes, what could be causing this that isn't purely thermodynamic? Since we are testing the same molecular compound in controlled conditions with consistent thermodynamic programs. What rules could be dictating the order and interaction of these particles on a localized scale, that is consistent across multiple tests, and seemingly inherent in the method of amorphisation?

As we can see, these docetaxel samples are polymorphs, true polymorphs. I don't know the intricacies of these specific polymorphic forms, but in the end they do not matter to the larger picture. The observable discrepancies between results like peak angles within the XRPD and Raman microscope, different pathways of degradation as seen by the FTIR while overall mass loss remains the same, and inconsistent temperatures in which phase transitions take place between the samples, show that these samples are polymorphs of each other. Beyond that the collection of measurements as a whole reconfirm and reinforce each others' results. Principles like these transcend the specifics of whichever chemicals you're using, and instead act as more universal rules to determine a crystal's polymorphism. All of the boxes are checked off in this case.

We can confirm conclusively that the Docetaxel shows Polymorphism throughout all of our measurement methods. Unfortunately the same cannot necessarily be said for our hydrochlorothiazide samples. Our DSC and TGA-FTIR results showed what look like characteristic differences; but the activation energy could not be found due to a lack of peak points, and our PDF data did not show any difference in peak locations. so the results on whether or not polyamorphism is occurring are inconclusive.

7 Chapter 7: Broader Perspectives

In order to confirm or deny polyamorphism within hydrochlorothiazide, we will need to test an x-ray PDF at further angstrom distances (our DESY test showed only slightly beyond the length of the molecule), so a WAXS run of the same forms may be required. In order to see activation energy, we likely need to run our TGA measurements to higher temperatures. It is likely that hydrochlorothiazide may not be the drug to confirm the existence of polyamorphism, due to the reasons highlighted in this paper. Further testing with other drugs will be necessary if the tests I have suggested don't lead to any conclusive results.

The unfortunate counterargument to the line of thinking justifying the different amorphous forms of HCT as polyamorphous, is that the amorphous forms that deviate most from the crystalline HCT when measured, both have some level of solvent in the mixture. The ball milled HCT is peppered with small bits of stainless steel; and the spray dried samples are bonded with ethanol, unavoidable with that method of amorphisation. The quench cooled samples, which have no solvent, on the other hand, are different from the crystalline form, yes, but not nearly as drastically. So it becomes increasingly unlikely that the force behind these differences is some sort of thermodynamic-independent "other" rule guiding the divergent behaviors of otherwise identical compounds, and it's instead more probable that the presence of other substances is what's driving everything. It is entirely possible that the double glass transition that we have observed is not a result of a miscibility gap between the two amorphous forms, but is rather the glass transition of whatever other compound is contaminating the system (making it somewhat heterogeneous). This would mean that solvatoamprphism is occurring, but not polyamorphism inherent to the structure and behaviour of the Hydrochlorothiazide molecule. Further tests need to be done to obtain a clearer picture.

Based on my thermocycling measurement (fig. 25), I would hypothesize that we transformed one polymorph of our DTX into another at stage 5. This would confirm that, while avoiding the decomposition point, we can relax one polymorph and steadily shift its amorphous form (as seen by changing "glass transition" temperatures) until a new polymorph recrystallizes. In order to test this theory, I believe we would need to undergo two tests: 1. Redoing the oscillation test, but this time with a correction and including more cycles. 2. Running a XRPD test on the same

temperature cycle and number of oscillations and plotting out the results along the 2theta axis. If the peak locations change, then that means that there was a change in polymorphs.

That being said, running further tests on this specific line of thought will be imperative for unlocking the ultimate rules behind crystal formation and growth. My only regret is that this was the last test done before data collection ended. Further research time and effort beyond this masters should be dedicated to this line of inquiry. I can say this with confidence.

The question still remains, why do systems behave the way they do even when there is no thermodynamic reason for it? If systems naturally trend towards chaos over time thanks to entropy, why would an amorphous substance (an inherently more chaotic system than its crystalline counterpart) always return to a rigid, ordered crystal given the time. What is this other driving force, and how can we quantify it? Answering these questions takes my thesis in the direction that I want it to go. I think in order to do that I will need to test on many different polymorphic substances. These are objects that are made up of the exact same materials but form and behave in very diverse ways, often based on initial circumstance. If we are able to crack this code, this would open up a wealth of possibilities in terms of analysis and prediction.

If we want to advance to automatic analysis and subsequent prediction of crystal growth and transformation, one option is to take many more repeated measurement, and then plug it into some sort of software with machine learning and simulation capabilities. The experamentalist's job is at that point is to determine which measurement methods actually contribute to an understanding and "deconstruction" of patterns present that directly dictate or indicate and quantify dictation of growth and transformation, and why. Beyond that a theorist or data analyst would use those specific data sets and parameters, and form an algorithmic software that could interpret and apply these principles. That is beyond the scope of this current master's obviously, but it would be useful next steps for continuing research in what truly seems (to me at least) to be a line of inquiry with rich scientific potential.

8 References

References

[1] National Library of Medicine. *Hydrochlorothiazide (Compound)*. 2020. URL: https://pubchem.ncbi.nlm.nih.gov/compound/Hydrochlorothiazide.

[2] *andas: pharmaceutical solid polymorphism*. URL: https://www.fda.gov/media/71375/download.

[3] Liana Vella-Zarb, Robert E. Dinnebier, and Ulrich Baisch. "The Devil is in the Detail: A Rare H-Bonding Motif in New Forms of Docetaxel". en. In: *Crystal Growth & Design* 13.10 (Oct. 2013), pp. 4402–4410. ISSN: 1528-7483, 1528-7505. DOI: 10.1021/cg400814a. URL: https://pubs.acs.org/doi/10.1021/cg400814a (visited on 08/22/2022).

[4] *DSC 214 polyma*. Publication Title: NETZSCH. URL: https://analyzing-testing.netzsch.com/en/products/differential-scanning-calorimeter-dsc-differential-thermal-analyzer-dta/dsc-214-polyma.

[5] Nikolaos S. Giannoulis, Heloisa N. Bordallo, and HeryEditors Mitsutake. "Identification of an Unknown Polymorph of Docetaxel and Evaluation of its Encapsulation into a Nanostructured Lipid Carrier". PhD Thesis. 2021.

[6] Brian C. Smith. *Fundamentals of fourier transform infrared spectroscopy*. CRC Press, 2011.

[7] Amy V. Margaris. "Fourier transform infrared spectroscopy (FTIR): Applications in archaeology". In: *Encyclopedia of Global Archaeology* (2014), pp. 2890–2893. DOI: 10.1007/978-1-4419-0465-2_343.

[8] A. Z. O. Materials. *Analyzing the Gas Phase Spectrum of Hydrogen Chloride with FT-IR*. 2018. URL: https://www.azom.com/article.aspx?ArticleID=15226.

[9] Jason Grebenkemper. *Powder X-ray diffraction*. Publication Title: Chemistry LibreTexts. Aug. 2020. URL: https://chem.libretexts.org/Bookshelves/Analytical_Chemistry/Supplemental_Modules_(Analytical_Chemistry)/Instrumental_Analysis/Diffraction_Scattering_Techniques/Powder_X-ray_Diffraction.

[10] *X-ray powder diffraction (XRD)*. Publication Title: Techniques. May 2022. URL: https://serc.carleton.edu/research_education/geochemsheets/techniques/XRD.html.

[11] L. Zaske, M.-A. Perrin, and F. Leveiller. “Docetaxel : Solid state characterization by X-ray powder diffraction and thermogravimetry”. In: *Le Journal de Physique IV* 11.PR10 (2001). DOI: 10.1051/jp4:20011035.

[12] D. Menon et al. “A thermal analysis study of the decomposition of hydrochlorothiazide”. In: *Instrumentation Science & Technology* 30.3 (2002), pp. 329–340. DOI: 10.1081/ci-120013511.

[13] “hydrochlorothiazide”. In: (). URL: http://www.thegoodscentscompany.com/data/rw1309061.html.

[14] Giuliana Gorrasi and Andrea Sorrentino. “Mechanical milling as a technology to produce structural and functional bio-nanocomposites”. In: *Green Chem.* 17.5 (2015). Publisher: The Royal Society of Chemistry, pp. 2610–2625. DOI: 10.1039/C5GC00029G.

[15] Khadijah Edueng et al. “Long-Term Physical (In)Stability of Spray-Dried Amorphous Drugs: Relationship with Glass-Forming Ability and Physicochemical Properties”. In: *Pharmaceutics* 11 (Aug. 2019), p. 425. DOI: 10.3390/pharmaceutics11090425.

[16] *Docetaxel*. Publication Title: ChemSpider. URL: http://www.chemspider.com/Chemical-Structure.130581.html.

[17] *XRPD on 3 samples*. Publication Title: XRPD on 3 samples. Mar. 2022.

[18] Siti kholijah Abdul mudalip et al. “Structures and Hydrogen Bonding Recognition of Mefenamic Acid Form I Crystals in Mefenamic Acid/Ethanol Solution”. In: *International Journal of Chemical Engineering and Applications* 4 (June 2013), pp. 124–128. DOI: 10.7763/IJCEA.2013.V4.277.

[19] Tuula Hakkarainen et al. “Smoke gas analysis by Fourier Transform Infrared Spectroscopy – Summary of the SAFIR project results”. In: *Fire and Materials* 24 (Mar. 2000), pp. 101–112. DOI: 10.1002/1099-1018(200003/04)24:23.3.CO;2-U.